Submitted to Annual Review of Nuclear Science

LBL-6570
Preprint

HIGH ENERGY INTERACTIONS OF NUCLEI

Alfred S. Goldhaber and Harry H. Heckman

March 1978

Prepared for the U. S. Department of Energy
under Contract W-7405-ENG-48

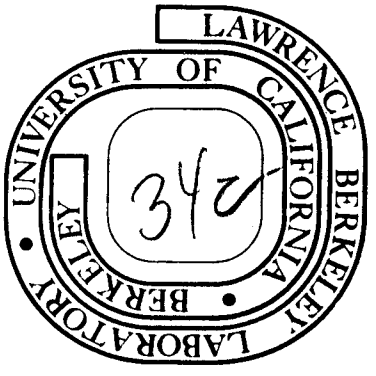

DISCLAIMER

HIGH ENERGY INTERACTIONS OF NUCLEI

Alfred S. Goldhaber*
Institute for Theoretical Physics
State University of New York
Stony Brook, New York 11794

and

Harry H. Heckman†
Lawrence Berkeley Laboratory
University of California
Berkeley, California 94720

* on sabbatical leave 1977-8

† Alexander von Humboldt Award, 1977-8

CONTENTS

1. INTRODUCTION

Nuclear physics and nuclear chemistry developed during the past half century as fields of research concerned with the nature of nuclear matter at or near equilibrium. The emergence in recent years of heavy ion accelerators with energies surpassing 100 A MeV (where A is the nuclear mass number) has opened the possibility of studying in the laboratory the effects of compressing nuclear matter to densities two or more times greater than normal while simultaneously "heating" the matter to temperatures in the 100 MeV range. This article is devoted to an assay of the present status of high energy nuclear collsion studies, and of the important questions which remain to be addressed.

A collision of two nuclei may be labeled by the impact parameter b. At one extreme is the case of maximum b, a peripheral or grazing collision, in which only one or a few nucleons leave the projectile or the target, and large, slightly excited projectile and target fragments remain. Such a process is widely supposed to be predictable in terms of conventional nuclear structure and collision theory. Indeed, plausible model approximations in this framework give a fair account of experimental data. Thus, from the viewpoint of a nuclear theorist, peripheral processes might be thought of mainly as a testing ground for conventional concepts. However, nuclear theory does not always attain that degree of precision and reliability required to make theoretical predictions useful for applications. For this reason, if no other, it has proved important to study such processes, especially projectile fragmentation, which plays a critical role in determining the composition of cosmic rays in proximity to the earth, and relating

that composition to the nature of cosmic ray sources.

At the opposite extreme in impact paramter is a central collision, in which the projectile and target overlap completely. Such collisions could produce the high densities and temperatures which might lead to important and perhaps surprising transformations of nuclear matter. It is obvious that theoretical predictions of such phenomena must be difficult and unreliable. However, the experimental analysis of central collisions is also a formidable challenge. First of all, there is not even an established criterion to identify a central collision. Secondly, assuming unusual effects occur during a stage of high compression, it is not clear how such effects would be manifested in the final distribution of reaction products.

The study of high energy nuclear collisions, then, has arrived at a natural "vista point" at which to appraise the progress already made and to set a future course. Fragmentation processes are well in hand, especially on the experimental side. Central processes have great potential, if we can find the right way to look at them.

The following section contains a brief historical review, starting with the early observations of cosmic-ray nuclear interactions. Also included are some kinematic terms, with definitions and motivations for their use, along with a description of accelerator facilities and a cursory outline of experimental techniques.

Section 3 is a description of the most mature branch of the subject, processes that leave significant near-projectile-velocity and near-target-velocity fragments.

Section 4 is a description of experiments which are not restricted to projectile or target fragments, and contains comparisons of data with conventional theoretical models representing the most conservative extrapolation of traditional nuclear and particle physics concepts. There is also a brief description of theoretical speculations about possible new phases of matter at higher-than-normal baryon density.

In both Sections 3 and 4, some theoretical comments are included in the experimental discussion, while others are put in a separate subsection.

Finally, in Section 5, we present some conclusions and suggestions for the future, hoping that these will stimulate other and better proposals from readers. To help compensate for omissions imposed by the brevity of this article, we list several other recent reviews on experimental or theoretical aspects of our subject.

2. PRIMER

2.1 History: Cosmic-Ray Period

Two independent works thirty years ago were forerunners of current approaches to high energy interactions between nuclei. Freier et al (1, 2) discovered $Z \geqslant 2$ components in the primary cosmic radiation, verifying a prediction by Alfvén (3), and opening the way to experimental studies long before high energy heavy-ion beams became available at laboratory accelerators. Meanwhile Feenberg & Primakoff (4) were led by the properties of the nucleon-nucleon tensor force to speculate that the familiar saturation of nuclear density might be overcome, and

tightly bound "collapsed" nuclei might occur in nature. In the past decade similar speculations based on various hypothetical mechanisms have appeared. Today the intriguing problem of high nuclear densities and the possible role of high energy nuclei in achieving these densities has become the most dramatic and difficult topic for experimental and theoretical investigation in this field.

Early studies of heavy-ion interactions in matter were primarily concerned with interaction mean-free paths and the production of nuclear fragments, as such data are most pertinent to the physics of cosmic rays. Here, the principal goal is to learn from the chemical and, eventually, isotopic composition of the observed heavy cosmic-ray nuclei, the conditions of their origin, acceleration mechanisms, and subsequent propagation. The astrophysically important information derived from heavy cosmic ray nuclei is described in comprehensive review articles by Shapiro & Silberberg (5), and Waddington (6), and the classic monograph of Powell et al (7), which has a wealth of information and pictorial examples of particle interactions in nuclear track emulsions.

2.1.1 QUALITATIVE CLASSIFICATION OF RELATIVISTIC HEAVY ION COLLISIONS

The pioneering cosmic ray work that pertains to the interactions of nuclei is given in a series of papers by Bradt & Peters (8-11), where one is introduced to the concepts of peripheral and central collisions between nuclei (9). In a peripheral collision, part of the projectile that overlaps the target nucleus may be sheared off. The remaining nuclear matter proceeds with its original velocity as fragment nuclei

of reduced charge and/or mass, alpha particles, and nucleons (10-12). Figure 1 is an example of a collision between an ^{40}Ar nucleus, kinetic energy T = 72 GeV (1.8 A GeV), with a Ag or Br nucleus in Ilford G.5 emulsion. This event shows the characteristics of both projectile and target fragmentation. The narrow forward cone of five He fragments indicates that a peripheral collision has taken place. The velocities of the He nuclei are approximately equal to the velocity of the incident ^{40}Ar (an example of persistence of velocities), and hence, correspond to low velocities (energies) in the projectile frame. In the laboratory, or target frame, the counterparts of such fragments are emitted as low-energy, heavily ionizing tracks, several of which are seen in this event. Note that a π^- meson is produced, comes to rest, and forms a three-prong star (Figure 1).

Figure 2 illustrates a central collision between a 1.8 A GeV-^{40}Ar projectile and a Pb target nucleus in a streamer chamber. In this case both nuclei are destroyed. Such an event involves high levels of excitation and the emission of a large number of secondary fragments. At least 63 particles, predominantly nucleons, light fragments, and pions (including six π^-) are produced in this particular event (Figure 2).

2.1.2 REACTION CROSS SECTIONS A semi-empirical "black sphere" expression for the reaction cross section of beam and target nuclei, with mass numbers A_B and A_T, respectively, introduced by Bradt & Peters (10) and extensively tested with nuclear emulsion detectors using cosmic ray nuclei $2 \leqslant Z \leqslant 26$ is

$$\sigma = \pi r_o^2 (A_B^{1/3} + A_T^{1/3} - \delta)^2. \qquad 2.1$$

The "overlap parameter" δ is meant to represent the diffuseness and partial transparency of the nuclear surfaces.

An assessment of the mean-free-path data for heavy cosmic-ray nuclei in emulsion by Cleghorn (13, 14) resulted in the following conclusions:

1) The overlap model accounts for the measured mean-free-path data for $2 \leqslant Z \leqslant 26$ to an accuracy of about 10-15% for $r_o = 1.2$ fm and $\delta = 0.5$. Because r_o and δ are coupled in Equation 2.1, these values are not unique.

2) The reaction cross sections of nuclei are essentially independent of energy from 0.1 to 30 A GeV.

3) The fragmentation parameters p_{ij}, the average number of i-type nuclei produced in the fragmentation of a j-type projectile, are also consistent with energy independence over this energy range. The errors in p_{ij} are typically 10-20% (5, 15).

Eisenberg (16) refined the Bradt-Peters approach, proposing a "grey sphere" model. Using a mean-free path $\lambda = 5$ fm of a nucleon in nuclear matter, of uniform density, he found a reduction of the geometric cross section due to transparency for $A_B = 25$ and $A_T = 64$ of 25%, and for $A_T = 207$ of 16%.

In the same paper, Eisenberg introduced what is now generally known as the abrasion-ablation model of nuclear collisions (17). He viewed fragment production as occurring in collisions that involved "cutting" of a part of the incident projectile, with removal of the

nucleons in the overlapping region (abrasion) and the subsequent evaporation of nucleons from the residual, excited pre-fragment (ablation).

Alexander & Yekutieli (18) and Aizu et al (19), noting that Equation 2.1 is independent of the nucleon-nucleon cross section in nuclear matter as well as the nucleon-density distributions of the colliding nuclei, calculated the reaction cross section σ_R for the nucleus-nucleus interaction at high energies from the optical model (20, 21). Alexander & Yekutieli presented their results as a function of σ_o, the effective nucleon-nucleon cross section in nuclear matter, and concluded that both the calculated nucleon-nucleus and nucleus-nucleus cross sections were in general agreement for values of σ_o = 30-40 mb. Their calculations showed that σ_R is not sensitive to σ_o. For example, a 10% change in σ_o results in only a 2% change in the σ_R for carbon projectiles. Thus, any energy-dependence of σ_o will be suppressed in σ_R.

2.1.3 REACTION PRODUCTS Although encumbered by low intensities and uncertainties in charge, mass, and energy determinations, experimental studies of nucleus-nucleus interactions using cosmic rays revealed important aspects of the high-energy interactions of nuclei. Early experiments were concerned with meson production by α-particles and heavier nuclei. Investigations by Jain et al (22) [α-particles and nuclei $Z \geqslant 6$, $7 \leqslant T \leqslant 100$ A GeV], Alexander et al (18) [$3 \leqslant Z \leqslant 8$, $T \geqslant 1.5$ A GeV], Tsuzuki (23) [$6 \leqslant Z \leqslant 8$, $T \approx 40$ A GeV], Rybicki (24)

[$Z \geq 3$, $T \geq 100$ A GeV], Abraham et al (25) [$Z \geq 2$, $T \geq 1000$ A GeV], and Andersson et al (26) [$3 \leq Z \leq 26$, $T \geq 1.7$ A GeV] are representative studies of shower-particle, i.e. fast meson and nucleon, production in cosmic-ray-heavy ion collisions over the energy range 1 to 10^3 A GeV.

Typical angular distributions of shower particles produced by cosmic-ray nuclei, $3 \leq Z \leq 26$, at kinetic energies greater than 1.7 A GeV (mean energy = 7 A GeV) are shown in Figure 3 (26). The principal feature of the angular distribution of shower particles is that they are composed of two main components: first, protons from the fragmenting projectile confined to a narrow cone, and second, pions and protons that have a wider distribution. Figure 3a shows the angular distribution of shower paricles $0 \leq \theta_{lab} \leq 80^\circ$, and Figure 3b gives a more detailed presentation at small angles $0 \leq \theta_{lab} \leq 12^\circ$. The curves show calculated angular distributions for pions, assumed isotropic in the nucleon-nucleon center of mass. The results of the work described above as well as other emulsion experiments by the University of Lund group (27-34) were in qualitative agreement with the hypothesis that the nucleus-nucleus interaction can be described as a superposition of independent nucleon-nucleon (18, 22, 24, 25), nucleon-nucleus (26), or α-α (23) collisions. However, notable discrepancies remained. (Figure 3)

1) The apparent recoil velocity, $\beta \approx 0.02$, of the residual target nucleus, as evident from the forward: backward ratios ≈ 1.4 for low energy ($\lesssim 30$ A MeV) fragments (black tracks, in emulsion terminology) is virtually independent of the mass of the projectile (18, 26, 28, 35, 36).

2) The spectra of energies, angles, and average multiplicities of black tracks, $\langle n_b \rangle$, are nearly the same for incident protons and heavy nuclei (28); $\langle n_b \rangle$ is usually considered to be a measure of the excitation energy transferred to the target nucleus.

3) For $T > 1.7$ A GeV, the mean multiplicities of pions $\langle n_\pi \rangle$ increase with energy [as $T^{0.4 \pm 0.08}$ between 10 and 40 A GeV (22)] and mass of the projectile, whereas the mean multiplicity of prongs with energies < 400 A MeV, $\langle n_h \rangle$, is nearly independent of these quantities (28).

4) Departures of the nucleus-nucleus interaction from the characteristics of the nucleon-nucleus interaction increase markedly as n_h increases, becoming most evident for AgBr interactions with $n_h \geq 28$ and for "central" collisions with $7 \leq n_h \leq 28$ and no $Z \geq 2$ projectile fragments produced (37, 34).

Considering the limited control over experimental conditions and the low statistics, precise understanding of the complex interactions of high energy nuclei could not be expected from cosmic ray experiments. Nonetheless, questions of basic importance were raised. For example, how is momentum transferred to nucleons and, in particular, helium, even when kinematically forbidden by models of quasi-elastic nucleon-nucleon or nucleon-alpha scattering (29)? Why does the structure of the projectile affect the charge (mass) distributions of its fragments (38, 39)? And finally, what are the possibilities for making and observing new modes of collective interaction in nuclear matter, only hinted at in the cosmic ray data on production of shower particles in highly

central and disruptive collisions?

Cosmic ray research has given us a preview of the physics of interactions between relativistic nuclei. We now focus our attention on this area of research, which came into existence with the development of relativistic heavy-ion beams at Princeton, Berkeley, Saclay, and Dubna in the early 1970's.

2.2 Glossary

As part of this primer we present a few definitions, mainly of kinematic quantities. For this discussion, we have referred to Ref. (40).

Momentum, p(GeV/c): $p = \beta\gamma E_o/c$, with $\beta = v/c$, $\gamma = (1-\beta^2)^{-1/2}$ and E_o the rest mass of the particle in GeV.

Rigidity, i) R (gauss-cm): $R = B\rho$, where ρ is the radius of curvature of a particle's trajectory in a magnetic field of strength B (the component normal to particle's momentum).

Rigidity, ii) R (GV): $R = pc/Ze$, with $pc = \beta\gamma E_o$ (GeV) and Z the number of units of charge carried by the ion. R is numerically equal to momentum per unit charge p/Z (GeV/c). R (GV) = 0.02998 R (kilogauss-cm).

Kinetic energy per nucleon, T/A (GeV): $T/A = (\gamma-1)E_o/A$, with A the mass number of the nucleus. Note that the definition implies trivially T = (T/A) A GeV; in other words, the energy of a nucleus with mass number A is the energy per nucleon, multiplied by A. Thus, the common usage giving energy per nucleon in GeV/A is incorrect; rather, the

proper unit is GeV. If atomic mass units are used, T/u is given in GeV, with $u = E_o/(0.91315016(26)\ \text{GeV})$.

Rapidity, y: For a particle in any system, $y = 1/2\ \ln\frac{E+P_{\|}}{E-P_{\|}} = \tanh^{-1}\beta_{\|}$, where E is the total energy, and $P_{\|}$ and $\beta_{\|}$ are the longitudinal momentum and velocity, respectively (c = 1). Use of the rapidity variable in place of velocity has the important property of relating two longitudinally moving frames by a simple translation along the rapidity axis. Therefore, distributions expressed in y have Lorentz-invariant shapes. At non-relativistic energies, $\beta_{\|} \ll 1$, $\beta_{\perp} \ll 1$, one obtains $y=\tanh^{-1}\beta_{\|} \approx \beta_{\|}$ and $P_{\perp}/E_o \approx \beta_{\perp}$. For an isotropic distribution in a system with y = 0, a contour plot of $P_{\perp}/E_o$ vs. y at low velocities will form concentric semi-circles about the origin. If the isotropic system is moving at β_c in the laboratory, the distribution will be the same, but centered on $y' = \tanh^{-1}\beta_c$.

At highly relativistic energies, one has $E \approx p$ and

$$y \approx 1/2\ \ln\frac{p+P_{\|}}{p-P_{\|}} = 1/2\ \ln\frac{1+\cos\theta}{1-\cos\theta} = -\ln\ (\tan\theta/2).$$

Thus, the shape of the distribution of particles in high-energy events, plotted in the variable $-\ln\ (\tan\theta/2)$, will be nearly independent of the velocity of the observation frame along the beam direction.

2.3 Heavy Ion Facilities and Experimental Techniques

We give a brief overview of high-energy heavy ion accelerators and the methods and techniques used in the experimental programs of these facilities. A full discussion is not only impractical but unwarranted,

considering the recent review articles by Grunder & Selph (41) on heavy-ion accelerators, Goulding & Harvey (42) on the electronic identification of nuclear particles, and Price & Fleischer (43) on particle tracks in solids, and the text by Fleischer, Price, and Walker (44) on tracks in solids, and Barkas (45) and Powell et al (7) on nuclear emulsions. An exposition of experimental techniques has been given by Stock (46) in his review of nuclear reactions between relativistic heavy ions.

2.3.1 HIGH-ENERGY HEAVY-ION ACCELERATORS: $T/A > 0.1$ GeV, $A \geq 4$

2.3.1.1 The Beginning By 1970-71 it had become evident that proton accelerators in the few GeV region such as the Princeton Particle Accelerator (PPA), and the Bevatron, had largely completed their missions in high-energy particle physics. There was also an increased awareness of new and beneficial applications of high-energy accelerators to fields other than high-energy physics (47). Longstanding interest in the use of high-energy heavy ions for biomedical research, as well as the realization that acceleration of heavy nuclei to relativistic energies would open a new field of nuclear research, were the principal scientific justifications for acceleration of heavy ions (48, 49). The first successful acceleration of relativistic heavy ions in the U.S. was achieved in 1971 at the PPA, a feat shortly followed at the Bevatron (50). Similar developments were taking place at Dubna (JINR), where acceleration of alpha particles in the synchrophasotron began in 1970. The possibility of using the ISR at CERN for heavy-ion experiments was also proposed (51).

2.3.1.2 Accelerators in Operation Table 1 summarizes the performance characteristics of synchrotrons that are accelerating beams of heavy ions, $Z \geq 2$ to energies $T/A \geq 0.1$ GeV. The closing of the PPA in 1972 made the Bevatron/Bevalac the only high-energy heavy ion facility in the U.S.

Major heavy ion facilities under construction or in the planning-proposal stages are:

1) Project GANIL, Caen, France. The maximum energy for this multi-accelerator system will be 8 A MeV for ^{238}U increasing to 0.1 A GeV for ^{12}C (53).

2) Numatron Project, Japan. A synchrotron and storage ring with energies from $\approx$ 0.7 A GeV (U) to $\approx$ 1.5 A GeV (Ne) (54).

3) Nuklotron Project, Dubna, USSR. A superconducting synchrotron with beam energies from 15-20 A GeV (55).

4) GSI, Darmstadt, Germany. First stage: A synchrotron with energies from 0.8 A GeV (U) to 2.0 A GeV (light ions). Second stage: 8-10 A GeV intersecting storage rings (56).

2.3.1.3 Bevalac The Bevalac, proposed by Ghiorso in 1971 (57, 49, 58), employs an 8.5 A MeV-heavy ion linear accelerator, the SuperHILAC, as an injector of heavy ions for the Bevatron, which then continues the acceleration of the ions to a maximum energy of 2.6 A GeV (for particles with $Z/A = 1/2$).

The SuperHILAC delivers beam intensities up to 10^{10}-10^{12} particles per pulse at a maximum pulse rate of 36 sec^{-1}. Because the Bevatron accepts particles for 500 μsec each 4 to 6 seconds, the SuperHILAC needs

only to divert a small fraction, $\approx 3\%$, of its duty cycle to the Bevatron. With two sources available the SuperHILAC can accelerate two different beams on a pulse-to-pulse basis, delivering one beam to the Bevatron while accelerating the other for low-energy heavy ion experiments. By use of time sharing, programs at the SuperHILAC and Bevatron can proceed largely independently of each other. Essential for operation of the Bevalac is complete computer control of all aspects of the acceleration process.

The requirements that the Bevatron accept only fully-stripped ions for acceleration means that the beam from the SuperHILAC must pass through a stripper foil at the maximum energy of 8.5 A MeV in order to produce the highest intensity of stripped ions. Both the stripping efficiency and losses due to charge-changing of the ions in matter increase as the charge of the ion increases, placing a practical limit on the heaviest element that can be accelerated. At the moment, this limit appears to be Fe. With a vacuum of 10^{-9} to 10^{-10} torr, and an upgraded SuperHILAC, the Bevalac would be able to accelerate partially-stripped ions. This is the basis for a proposal to install a vacuum liner in the Bevalac and a third injector in the SuperHILAC to produce high intensity uranium beams at 1.1 A GeV (U^{+72}) (59). With such an improved system, the use of partially-stripped ions would permit efficient acceleration and extraction of particle beams at energies as low as 35 A MeV, giving the Bevalac an extraordinary range of beam masses and energies.

2.3.2 EXPERIMENTAL TECHNIQUES Experiments in high-energy heavy ion physics, because of their wide ranges in particle mass, charge, and energy, necessarily involve the application of particle detection methods from both low-energy nuclear and high-energy particle physics. The added dimension of high multiplicities of highly-charged nuclear fragments, nucleons, and mesons that often occur in high-energy collisions between nuclei offers formidable technical and interpretative problems--problems that are now only in embryonic stages of solution.

The techniques used in any particular experiment correlate quite well with the rapidity variable. Low values of rapidity are characteristically target-related, so that traditional methods of nuclear physics are applicable, e.g. particle identification by (ΔE-E) and time-of-flight (TOF) (60), with measurements over practically 4π steradians. Experiments in the realm of high rapidity, associated with projectile fragmentation where the beam-velocity fragments are emitted within a few degrees of the incident projectile, require the application of high energy techniques, magnetic spectrometers, and large beam-transport systems (61, 62). Such experiments therefore may incorporate measurements of dE/dx, rigidity, TOF for slow particles, Cerenkov radiation (for relativistic particles) and particle trajectories, as well as use of streamer chamber (63) or other multiple-track, electronically-triggered detectors. Visual methods of detection by emulsions, plastics and AgCl monocrystals (64, 65) are also important in heavy-ion experiments because of their wide range of sensitivities, 4π-geometry, versatility, and small demands for beam time.

To date, experiments have largely been designed to emphasize the low and high rapidity regions, with only limited capabilities for excursions into the central regions and to high transverse momenta. Because the measurements of total kinetic energy by range are rapidly curtailed by the finite size of the detectors and losses due to nuclear interactions, experiments that pertain to particles of intermediate energy, $\gtrsim 0.2$ A GeV, will tend to use dE/dx, rigidity, TOF and/or Cerenkov radiation for particle identification. The minimal requirement here is to design magnetic spectrometers of modest size to measure particle rigidities (p/Z) and, by rotation about the target, to measure particle production over a wide range of angles (66).

The principal feature that distinguishes heavy-ion from typical high energy physics experiments is the presence of a large range of particle charges, Z. Although a measurement of $dE/dx \approx Z^2 f(\beta)$ alone is sufficient to distinguish elements at relativistic velocities, technical problems arise when charge identification and accurate time measurements must be made over a broad range of nuclear charges and velocities. In such cases, an amplifier-discriminator system is required which first samples a signal to find whether it is large or small, and then selects the appropriate sensitivity for accurate signal measurement.

3. NUCLEAR FRAGMENTATION

Fragments observed to have low velocities ($\beta \lesssim 0.3$) in the rest frame of a projectile or target nucleus may be considered "spectators"

of a high energy collision. The high rapidity of projectile fragments in the laboratory is important because it permits measurements of fragment momenta that correspond to very low velocities in the projectile frame (even zero)—measurements not possible with traditional target fragmentation experiments because of the inability of the fragments to escape finite-size targets.

3.1 Projectile Fragmentation

Single-particle inclusive experiments form the basis of our information on projectile and target fragmentation. In these experiments, the reaction investigated is B + T → F + X, where B and T represent the beam and target nuclei, F is the (single) detected fragment nucleus, and X refers to all other (undetected) reaction products.

Two general terms, discussed in both high-energy particle physics and low-energy nuclear physics, have wide, though not universal, application to these data. In the high-energy language, the first feature is called "limiting fragmentation" (67) or "scaling" (68). This means that a distribution of products with finite energies in the rest frame of projectile or target approaches a limiting form as the bombardment energy increases. Practical tests of limiting fragmentation demonstrate that, in a given range of bombarding energies, a particular distribution shows negligible change. The second term is "factorization" (69). This means that the cross section for production of a particular projectile fragment may be written as the product of a factor γ_T depending only on the target and a factor γ_B^F depending only

on the beam and fragment. Obviously the roles of projectile and target may be interchanged to describe target fragmentation. In the language of nuclear physics, both factorization and limiting fragmentation are examples of Bohr's independence hypothesis for decay products of a "compound nucleus" (70). This amounts to the statement that the object emitting a fragment keeps little or no memory of the formation or excitation mechanism which produced it. Of course, these concepts are not automatically valid, but must be tested by experiment. It appears that fragment-velocity distributions do assume a limiting form over successively larger domains of velocity as collision energy increases. On the other hand, as common sense would suggest, factorization seems to hold only for products of grazing collisions, and in particular is untrue for total cross sections.

3.1.1 NUCLEUS-NUCLEUS CROSS SECTIONS Measurements of the total nucleus-nucleus cross sections, σ_{TOT}, using "good geometry" techniques, have been made by Jaros et al (71) for each of the 32 possible target/projectile/energy combinations of the light nuclei p, d, ^{4}He, and ^{12}C at 0.87 and 2.1 A GeV. The total cross sections σ_{TOT} (A,A) at 2.1 A GeV for identical target and projectile masses are shown in Figure 4. The data are well accounted for by Glauber theory. Another possible A-dependence of σ_{TOT} would be the factorization form, σ_{TOT} (A,A) = σ^2_{TOT} (pA)/σ_{TOT} (pp), which obviously disagrees with the data. (Figure 4)

The inelastic cross sections σ_{IN} for reactions initiated by d, ^{4}He, and ^{12}C are found to be independent of beam energy, with σ_{IN} (0.87 A GeV) = (1.00 ± 0.01) σ_{IN} (2.1 A GeV) (71).

Reaction, or more precisely, transmutation cross sections σ_R for projectile nuclei including ^{4}He, ^{12}C, ^{14}N, ^{16}O, and ^{40}Ar have been measured at $\approx$ 2.0 A GeV (72-75), and at 0.15-0.2 A GeV (76) in emulsion, and for a variety of target materials, H through U, with a tungsten-scintillator calorimeter (77) and an elemental transmission detector-telescope system (78). In general, these techniques are sensitive only to interactions that involve changes in the charge Z of the projectile, i.e. $\Delta Z \geqslant 1$. When supplemented by an estimate of neutron stripping, the resultant cross section is σ_R ($\Delta A \geqslant 1$), hence the term transmutation. Within their respective errors, the mean-free-path lengths in emulsion are consistent with energy independence down to 0.15 A GeV (76). The σ_R values measured by Lindstrom et al (78) for ^{12}C, ^{16}O, and ^{40}Ar, T/A $\approx$ 2 GeV, gave the first experimental evidence that the Bradt-Peters overlap parameter δ is not constant, but depends upon $A_{min} = \min (A_T, A_B)$. They found that for $r_o = 1.29$ fm and $\delta = 1.0 - 0.028A_{min}$ (with $\delta = 0$ for $A_{min} \gtrsim 30$), Equation 2.1 fits σ_R for all beam and target combinations to 10%. Optical model estimates for σ_R (79, 80) show the same pattern as the experimental data (72).

3.1.2 ISOTOPE PRODUCTION The major feature of the isotope production cross sections from fragmentation of relativistic projectile nuclei, T = 1.05-2.1 A GeV, is that they are independent of energy, and are factorable (81-84, 62). The 0-degree fragmentation cross sections of ^{12}C and ^{16}O projectiles, T = 1.05 and 2.1 A GeV, have been measured by Lindstrom et al (82) for all nuclear fragments, $1/3 \leqslant Z/A \leqslant 1$ for targets H to Pb. Some 470 cross sections for 35 isotopes were

determined. An analysis of the systematics of the measured cross sections leads to the following conclusions:

1) σ_{BT}^{F} is energy independent: σ_{BT}^{F} (2.10)/σ_{BT}^{F} (1.05) = 1.01 ± 0.01 for all fragments (F) of ^{12}C (B). Limiting fragmentation is satisfied.

2) Factorization, i.e. $\sigma_{BT}^{F} = \gamma_{B}^{F}\gamma_{T}$, is valid to a high degree. Exceptions are apparent for H and possibly He (85) targets, and one-nucleon loss cross sections in high-Z targets. The latter is explained qualitatively as Coulomb dissociation of the projectile in the target's electric field: the projectile is excited to the giant-dipole resonance and decays by particle emission (86).

3) A target factor $\gamma_{T} \propto A_{T}^{1/4}$ accounts for the data to ≈ 10%, as does the form $A_{T}^{1/3}$ + constant.

The functional forms of γ_{T} are essentially geometrical in character, and imply that projectile fragmentation results from peripheral, i.e. large impact-parameter, interactions. Other significant features of the fragmentation cross sections are: a) no nucleon-pickup isotopes are observed ($\sigma \leqslant 10\mu b$), b) from 30% (Pb target) to 90% (H target) of the beam charge is accounted for by summing the fragmentation cross sections, and c) nuclear structure effects of both projectile and fragment are evident, often dominant, in establishing the isotope production cross sections.

3.1.3 MOMENTUM DISTRIBUTIONS The isotope production cross sections at beam energies ⩾ 1 A GeV are consistent with factorization and energy independence. This suggests that the momentum distributions of

fragments in the projectile rest-frame should also exhibit independence of target structure and beam energy. These limiting conditions are, in fact, met to better than 10% accuracy for fragmentation products of ^{12}C and ^{16}O (87) and ^{4}He (83, 62), for fragment momenta $p \lesssim 400$ MeV/c (projectile frame), at beam energies $T \geqslant 1.05$ A GeV. Evidence for energy-dependent changes in the fragment-momentum spectra from ^{4}He at 0.4 A GeV (62) indicates that the fragment distributions become limiting somewhere between beam energies 0.4 and 1.05 A GeV.

The rigidity ($P_{\|}c/Ze$) spectrum shown in Figure 5 is typical of all such isotopic spectra from the 0-degree fragmentation of ^{12}C at 1.05 and 2.1 A GeV and ^{16}O at 2.1 A GeV. (Figure 5) The rigidity distribution of each isotope is peaked near the beam velocity, and the widths of all isotope peaks are about the same. In the rest frame of the projectile, the longitudinal momentum distributions show a Gaussian dependence on $P_{\|}$, Figure 6. (Figure 6) Irrespective of projectile, beam energy $\geqslant 1.05$ A GeV, and target nucleus, the $P_{\|}$-distributions for all fragments from ^{12}C and ^{16}O, with the exception of protons, are characterized by:

1) A Gaussian shape, with rms widths $\sigma(P_{\|}) \approx 50$ to 200 MeV/c and values of $\langle P_{\|} \rangle \approx -10$ to -130 MeV/c. The latter show that the mean velocites of the fragments are less than that of the projectile, evidence of nuclear "friction".

2) RMS widths $\sigma(P_{\|})$ and $\sigma(P_{\perp})$ that are equal to an accuracy of 10%, consistent with isotropic production of fragments in a frame moving at $\langle \beta_{\|} \rangle \approx -\langle P_{\|} \rangle / E_o$ in the projectile frame.

3) $\sigma(P_{\|})$ and $\langle P_{\|} \rangle$ that are a) independent of target mass and beam energy and b) dependent on the masses of the beam B and fragment F.

These observations satisfy limiting fragmentation and factorization. The general trend of the measured $\sigma(P_{||})$ is reproduced by the expression $\sigma(P_{||})$ (B,F) = $2\sigma_0[F(B-F)]^{1/2}B^{-1}$. The parabolic dependence of $\sigma(P_{||})$ on fragment mass arises from a variety of theoretical approaches, all dependent on simple postulates including conservation of momentum (70, 88, 89). Although the parabolic shape reproduces the general trend of the data, deviations indicate the importance of fragment structure and final-state binding energy effects on $\sigma(P_{||})$ (90).

Fragmentation of ^{4}He has been studied in the reactions ^{4}He + (C, CH_2, Pb) → (p, d, ^{3}He, ^{4}He) + X at beam energies 0.4, 1.05, and 2.1 A GeV. Extending the work of Papp et al (83), Anderson (62) measured fragment momenta over the intervals $0.5 \leqslant p \leqslant 11.5$ GeV/c and $0 \leqslant \vartheta_{lab} \leqslant 12^\circ$, giving $P_\perp$ up to 600 A MeV/c.

The $P_\perp$-distributions of beam-velocity protons from ^{4}He on a ^{12}C target are presented in Figure 7 for beam momenta 0.93, 1.75, and 2.88 A GeV/c. They show no dependence on beam momenta to an accuracy $\lesssim 10\%$. The momentum distributions for all fragments, p through ^{3}He, produced with $P_\perp = 0$, are asymmetric in the projectile rest frame. This asymmetry is observed at each beam momentum, and is due, in part, to longitudinal momentum transfer between the projectile and target. Angular distributions in the projectile frame also show forward-transverse asymmetries. Distributions of $P_\perp$ are broader than those of $P_{||}$, suggesting contributions by hadronic scattering processes. The same conclusion comes from an experiment on the inclusive production of He in the reaction ^{4}He + p → ^{3}He + X measured with incident ^{4}He at 6.85 GeV/c

(1.02 A GeV) (91), where the kinematics of ^{3}He-production are dominated by the quasi-elastic scattering of the target proton on the ^{3}He-component in the ^{4}He projectile, the remaining neutron acting as a spectator. (Figure 7)

Momentum spectra of fast pions, viewed as projectile fragments, also show limiting fragmentation down to beam energies of 1 A GeV (83, 55). This is shown in Figure 8 (83), where the invariant cross sections for π^- production at $\theta_L = 2.5^\circ$ are plotted as a function of the scaling parameter $x' = k_{||}^*/k_{||}^*(max)$, with $k_{||}^*$ the longitudinal momentum in the center of mass, and $k_{||}^*(max)$ the maximum value allowed by energy and momentum conservation. The scaling property is demonstrated for each projectile type by the fact that the pion yield depends on x' only, and not on the energy of the projectile. The data show excellent agreement with a model of Schmidt & Blankenbecler (92). (Figure 8)

Frankel et al (93, 94) have observed fast backward fragments from heavy targets bombarded by protons. Their results, as well as those from fast forward projectile fragments, indicate the presence of short-range structure in the nuclear wave function. There have been several semiphenomenological approaches to parameterize these data, each based on a different picture of the collision process. At one extreme is the notion of the "cumulative effect", in which the effective projectile is supposed to be a compact object of mass larger than a nucleon (95-97). By kinematics alone, this permits fast forward fragment emission. A second approach is to assume a spectrum of nucleons with high virtual three-momentum inside the projectile. The scattering process releases this momentum. For an exponentially falling virtual momentum spectrum, good agreement with target fragment-

ation data is obtained (94). Finally, a relativistic analogue of this notion, the parton model, relates the distribution of observed x' values to a vertex function, that is, a generalization of a momentum-space wave function. Simple powers of $(1-x')$ give good fits to light projectile fragmentation (92). The different approaches actually give similar parameterizations of data, and are probably closer conceptually than their presentations suggest.

3.1.4 FRAGMENTATION REACTIONS AT NON-RELATIVISTIC ENERGIES Cross sections for production of projectile fragments He through N in ^{16}O-emulsion nucleus interactions at 0.15-0.2 A GeV were measured and compared with those measured at 2.1 A GeV (76). The cross sections for Be, B, C, and N were the same within experimental errors (10-25%), but production of Li and He were found to be larger at 0.2 than at 2.1 A GeV, up to a factor of 2.8 ± 0.4 for Li. Differences in the topology of the ^{16}O interactions leading to the production of Li and He fragments at these energies were also observed. For example, the production of Li via $^{16}O \rightarrow Li + Li + X$ occurs in about 25% of the Li-producing reactions at 0.2 A GeV, but is unobserved (in approximately 2800 interactions) at 2.1 A GeV (74, 75, 72). This is a consequence of increased excitation energies at 2.1 A GeV beam energy, which suppresses multiple-emission of light nuclei.

Unexpectedly, the cross sections and kinematics of peripheral collisions between ^{16}O at 0.315 GeV (0.02 A GeV) on target nuclei $94 \leqslant A_T \leqslant 232$ show remarkable similarities to the fragmentation of ^{16}O

projectiles at 33.6 GeV (2.1 A GeV) (98-101). The relative isotope yields are essentially target independent, and within experimental errors, the relative yields from ^{16}O on ^{208}Pb are identical to those measured at 2.1 A GeV (98). Differences in the isotopic production cross sections are observed, however, the trends being toward lower production cross sections for neutron-deficient isotopes at the lower energy. The angular distributions and energy spectra in the excited projectile frame are similar to those seen at Bevalac energies (100, 101).

3.2 Target Fragmentation

Cross sections for fragmentation of light nuclear targets ($A \leqslant 27$) by proton beams (see Ref. 102) and by alpha beams (see Ref. 85) are in generally good agreement with projectile fragmentation data for comparable energies. The fragmentation of heavy target nuclei ($A \geqslant 67$) leads to a wide range of fragment residues, the products of spallation and nuclear fission. The large number of identifiable radionuclides (up to 76 for ^{238}U) gives a good statistical basis for comparing the mass and charge distributions for different target/projectile/energy combinations, as a means for revealing new interaction mechanisms that may arise.

Radioanalytical studies have been done on the energy dependence of ^{4}He-induced spallation of niobium, $0.08 \leqslant T \leqslant 0.22$ A GeV (103). Heavy-ion irradiations of Cu have included ^{4}He at 0.18 A GeV (104), ^{12}C at 2.1 A GeV (105), ^{14}N at 0.28 A GeV (106), and ^{40}Ar at 1.8 A GeV (107). Target-dependent data are available from radioanalytical experiments on

the reactions of 2.1 A GeV-^{12}C nuclei with Ag (108), Au, Pb (109), and U (110). Track detectors have been used to study fission reactions induced by ^{14}N-bombardment of U, Bi, Au, and Ag at energies 0.14, 0.28, and 2.1 A GeV (111).

The principal result of these spallation experiments is, except for some non-fission products of U (110), the remarkable similarity of the mass-yield and charge-dispersion (at each fixed mass) curves for all projectiles, including protons (105-108). Cumming et al found no detectable difference in the shapes of the charge-dispersion curves for fragment masses $37 \leqslant A_F \leqslant 61$ from the spallation of Cu by 25 GeV-^{12}C (105) and by ^{14}N and protons, both at 3.9 GeV (106). The 3.9 GeV-^{14}N and proton data are compared in Figure 9. Illustrated here is evidence for factorization and, because of the identity of the 3.9 and 29 GeV charge-dispersion curves, limiting fragmentation. This implies that peripheral reactions are the dominant source for these (mid-mass) spallation products of Cu. (Figure 9)

Because the observed spallation products result from all collision-impact parameters, central collisions also contribute to the mass distributions. For central collisions, however, factorization fails and the yields from such collisions will depend on the mass of the projectile. This may account for the observation that some light fragment yields (^{3}He, ^{7}Be) do not factor (107, 108). Loveland et al (110) observed that the interaction of 2.1 A GeV-^{12}C with U produces a particularly large enhancement in the mass yield curve in the region $160 \leqslant A_F \leqslant 190$, a feature completely absent in the 28-GeV p + U mass-

yield curve. Such an effect must be a consequence of non-peripheral collisions. There is more evidence for contributions of non-peripheral collisions to target fragmentation. Westfall et al (102) remarked on the appearance of a "high temperature", roughly 15-MeV, Maxwellian energy distribution of fragments from nuclei bombarded by protons. This high temperature component becomes increasingly conspicuous (relative to the $\approx$ 8-MeV Maxwellian characteristic of light nucleus fragmentation) as target mass increases. The effective temperature rises above 15 MeV as projectile mass increases (112,60), showing a breakdown of factorization.

Heavily ionizing "black" tracks (momenta $p \lesssim 0.25$ A GeV/c) from relativistic interactions in nuclear emulsion are attributable to target fragmentation (34, 73, 113, 114). The rapidity distributions of such fragments (assumed to be protons) from AgBr under bombardment of ^{4}He, ^{16}O, and ^{40}Ar projectiles at $\approx$ 2 A GeV are found to be Maxwellian (114). To within the errors of the experiment, the values of $\langle y \rangle$ and the standard deviation σ_y are independent of projectile mass, the mean of all distributions being consistent with $\langle y \rangle = 0.014 \pm 0.002$ and $\sigma_y = 0.082 \pm 0.001$, the latter corresponding to a temperature $\tau = 6.3 \pm 0.2$ MeV. These results are impressively close to values of $\langle \beta_{||} \rangle$ and τ obtained from the momentum spectra of projectile fragments (87).

The near-constancy of the CM-velocity $\beta_{||}$ of the emitting system has been demonstrated for a variety of projectiles, π^-, p, and heavy ions, when the projectiles are relativistic, and fragment ranges are in the interval 0-4 mm (tabulations are given in Refs. 28, 36, 114). The

velocity $\beta_{\|}$ is not an invariant feature of heavy ion collisions, however, since it has been found to increase when a) the fragment range (energy) is increased (114), b) the amount of charge, ΔZ, lost by the target nucleus, i.e. the degree of dissociation, increases (74), and c) the projectile energy decreases (115, 113, 60, 116, 117, 100, 101). Similar phenomena are observed in ^{14}N-induced fission reactions where the binary fission and single (energetic spallation) tracks show increased angular asymmetries as either the beam energy, or mass of the target, decreases (111).

A two-step kinematic model (118) is applicable to these observations (100, 101). In this model, target fragmentation proceeds via a) $B + T \rightarrow B^* + T^*$, b) $T^* \rightarrow F + X$. From the conservation of energy-momentum, the recoil velocity of the target is given by the expression, valid for recoil $\ll$ excitation $\ll$ nuclear rest energies,

$$\langle \beta_T \rangle \approx (\gamma E_T^* + E_B^*) \ (M_T \beta \gamma)^{-1}, \qquad (3.1)$$

with β the beam velocity, $\gamma = (1 - \beta^2)^{-1/2}$, E_T^* and E_B^* the respective excitations of target and beam nuclei, and M_T the target mass. Equation 3.1 explains the following qualitative features of the cited data: a) $\langle \beta_T \rangle$ is independent of M_B (factorization); b) for given values of E_T^* and E_B^*, asymmetry anticorrelates with target mass; c) given $E_T^* \ll E_B^*$, i.e. low target excitation, asymmetry anticorrelates with beam momentum, and d) asymmetry correlates with energy deposition in the collision.

3.3 Theoretical Aspects

The phenomena of nuclear fragmentation have been analyzed by a number of theoretical techniques which are well tested in familiar domains of nuclear and particle physics. Such analyses have given successful explanations of available experimental data, ranging in precision from percent-level accuracy for total cross sections to semi-quantitative or qualitative descriptions of fragment production rates and momentum distributions.

3.3.1 TOTAL CROSS SECTIONS The high energy model of Glauber (21), which has been remarkably successful in describing nucleon-nucleus cross sections (119), supplies a physically reasonable and computationally tractable framework for deducing nucleus-nucleus cross sections also (120). The fundamental approximation of the model is that during the collision any projectile-nucleon target-nucleon pair wave function suffers a complex phase shift depending only on the nucleon-nucleon relative impact parameters. Therefore, the nucleus-nucleus wave function is multiplied by a phase factor $\exp [i\Sigma\chi_{jk}(\underline{b}_{pj} - \underline{b}_{tk})]$ where the sum goes over all pairs of nucleons. For a given nucleus-nucleus impact parameter $\underline{b}$, the above phase factor averaged over projectile and target ground-state nucleon distributions yields $\exp [i\chi(\underline{b})]$, the survival amplitude at impact parameter $\underline{b}$. Huyghens' construction gives the small q elastic scattering amplitude (q = momentum transfer) as proportional to the Fourier transform of $\{1 - \exp[i\chi(\underline{b})]\}$, and hence by the optical theorem the total and

reaction cross section formulas,

$$\sigma_T = 2\mathrm{Re}\int d^2b\{1 - \exp[i\chi(\underline{b})]\} \quad . \tag{3.2}$$

$$\sigma_R = \mathrm{Re}\int d^2b\{1 - |\exp[i\chi(\underline{b})]|^2\}. \tag{3.3}$$

Thus, given sufficiently accurate nucleon distributions inside each nucleus, and given $\chi_{jk}(\underline{b}_{pj} - \underline{b}_{tk})$ (which may be obtained by fitting nucleon-nucleon scattering data), one may compute the cross sections by integration. As Figure 4 shows, the results for light nuclei are in good agreement with experiment. The actual calculations require inclusion of Coulomb phase shifts, since the Coulomb parameter $\alpha Z_1 Z_2$ can be quite large. The model is physically reasonable, since results are sensitive mainly to interactions of surface nucleons. For these nucleons the approximations a) that their internal motion during the collision can be neglected and b) that they interact as if free are most plausible. Under some additional approximations, Glauber's model becomes equivalent to the optical model, which therefore gives the same results when valid (120).

3.3.2 FRAGMENTATION High energy reactions which deposit small amounts of energy in nuclear residues are naturally described as occurring in two stages--a fast collision which may lead to knock-out of one or more nucleons, followed by de-excitation on a time scale characteristic of internal nuclear motion (70). Calculational approaches involving high-energy approximations, such as the Glauber model or the intranuclear cascade model (121), may be used to describe

the first stage. In the cascade model, individual projectile and target nucleons move at uniform velocities between collisions with other nucleons (different particles, like pions, may also be included). The position and outcome of each collision in a given cascade are determined by random sampling of probabilities derived from the elementary cross sections. Thus, even for a fixed nucleus-nucleus impact paramter it may be necessary to follow many cascades in order to obtain a probability distribution for configurations at the end of the fast stage. The energy deposited by the cascade in a "spectator" residue gives the input for the second stage, in which fragments "evaporate" from the residue, assumed to be in rough thermal equilibrium. While there is an extensive literature on cascade calculations for protons incident on nuclei, attempts to deal with complex-nuclear projectiles have begun only recently, and with an emphasis on products other than projectile or target fragments (122).

The cascade calculations, once they become available, should be most appropriate for describing the high temperature component of fragment distributions, as well as examples of isotope production which do not exhibit factorization. That is, processes which involve large overlap of projectile and target are likely to be insensitive to quantum interference effects, so that a minimally quantum-mechanical scheme may be used to describe them. Indications from the proton data (102) are that these nonfactorizing processes exhibit limiting fragmentation for bombardment energies greater than a few A GeV.

In contrast to the above, the properties of the "low temperature

component" and of fission (which also involves very small energy deposit), namely factorization and limiting fragmentation at about 20 A MeV bombardment energy, invite a different, more quantum-mechanical approach. Hüfner and collaborators (123) have given the most systematic treatment to date, using Glauber theory to describe the fast stage. In this approach, the survival factor $\exp[i\Sigma\chi_{jk}(\underline{b}_{pj}-\underline{b}_{tk})]$ is treated as an operator on the projectile and target nuclear wave functions. As nuclear overlap increases with decreasing impact parameter, the survival factor differs more from unity, so that higher states are excited. Even at a given impact parameter, the excitations of projectile and target are likely to be correlated. If the exact nuclear Hamiltonian were known, the result of the fast stage could be used to give the initial condition for the slow evolution of the excited nucleus. Lacking this, one must make further approximations to describe the second stage, and improvement in these approximations may be the most fruitful area for further developments in the theory of low-energy processes leading to nuclear fragment emission.

In its domain of applicability, $T \gtrsim 1$ A GeV, the Glauber approach automatically implies limiting fragmentation at least to the extent that the nucleon-nucleon cross section is constant. Approximate factorization for light-projectile fragmentation is also a natural consequence, since highly peripheral interactions primarily involve direct contact of one or a few nucleon pairs in a localized overlap region and hence the resulting excitations are insensitive to the shape of the other nucleus. It should be mentioned that another aspect of factorization, namely noncorrelation of projectile and target

excitations, has been little studied in theory or experiment.

Projectile fragment momentum spectra and relative isotope frequencies both indicate an effective "temperature" of 8-10 MeV (87, 100). The Gaussian momentum spectra could be due to a combination of factors, the approximate validity of harmonic oscillator shell model wave functions, and the fact that several nucleon momenta are being added randomly, resulting in almost instant emission of the fragment. On the other hand, the appearance of a Boltzmann factor in the frequency distribution of modes of fragmentation (124) suggests a slower process, in which the mean energy deposited is distributed over many degrees of freedom before fragment emission occurs. From this point of view, it would be interesting to study fragmentation of heavier projectiles by unexcited targets, to see if the (presumably similar) local energy deposit is spread out more, resulting in lower effective temperatures.

4. GENERAL PROCESSES

Particles not identifiable with projectile or target fragmentation are deemed to come from general processes. Experimental studies of such processes therefore require sensitivity not only to target and projectile regions of rapidity, but also to intermediate rapidites and large transverse momenta. In this chapter we consider single-fragment production in the near-target region, where target emission remains distinctive, but where effects of the projectile nucleus are evident, and then go on to the intermediate region, where fragment emission can no longer be identified with either target or projectile.

4.1 Near-Target Rapidities

Information on fragment production in the near-target regions has come from studies on the emission of fast, light nuclei, $Z \leq 2$, $T \lesssim 250$ A MeV, from interactions of heavy ions in emulsions (76, 113, 74, 73, 114, 116) and AgCl-monocrystalline detectors (115, 117) at beam energies $0.1 \lesssim T \lesssim 4.2$ A GeV, from measurements of the energy and angular distributions for fragments produced in the reaction 2.1 A GeV-^{12}C + Au $\rightarrow$ Z, with $5 \leq Z \leq 9$ (125), and from a comprehensive study of the single-fragment inclusive reactions $\begin{matrix} Ne \\ He \end{matrix} + \begin{matrix} U \\ Al \end{matrix} \rightarrow F + X$ at selected beam energies T = 0.25, 0.40, and 2.1 A GeV (60). In the experiments of Gosset et al (60), the detected fragments were protons through nitrogen with energies $30 \leq T \leq 150$ A MeV and angles $25^\circ \leq \theta_L \leq 150^\circ$.

Some qualitative features of fragment emission in the near-target region are:

1) The angular distributions for the hydrogen and helium isotopes are smooth, and exhibit forward peaking that increases with mass and energy of the fragment (125, 60, 113, 73, 114, 116), and with decreasing beam energy (60, 115, 117, 113, 116).

2) Proton production is predominant, especially for $\theta_L > 90^\circ$, since other fragment energy spectra fall more steeply with increasing angle. The cross sections for ^3He are enhanced at high fragment energies, characteristic of neutron-deficient isotopes (60).

3) The spectra of all fragments deviate from exponential (evaporation-like) spectra, tending to power-law distributions (125, 60, 126, 74, 113).

4) The production of light fragments, e.g. ^{3}He, is dependent on the target. The angular distributions are nearly independent of the projectile (60).

5) The emission of fast He nuclei, $10 \leq T \leq 250$ A MeV, is associated with high excitation energies (74, 60). Up to seven target-related He nuclei per interaction have been observed in emulsion events, with combined kinetic energies often exceeding 1 GeV (33).

Figure 10 shows contours of the invariant cross sections $p^{-1}d^2\sigma/dEd\Omega$, from Gosset et al (60) for the reaction $^{20}Ne + U \rightarrow {}^3He + X$, plotted in the rapidity versus $P_\perp/A_F$ plane for each bombarding energy indicated. The heavy contours are identified by the $\log_{10}$ of the invariant cross section. The spacing between contours corresponds to a constant factor in the cross sections. Note that at 2.1 A GeV, the contours are well separated from $y_{proj} = 1.84$, and the identification of target-related production of ^{3}He is quite clear. At 250 A MeV, the smaller rapidity gap between the target and projectile ($y_{proj} = 0.71$) does not allow such clean separation between the target and projectile regions. To interpret these patterns, recall that for fragments emitted isotropically from a unique moving source, the contours will center about the rapidity of that source. The data show that no such unique source exists. At the lowest value of $P_\perp$, the apparent sources have rapidities $y \lesssim 0.1$. As $P_\perp$ increases, the shifts in the centroids of the contours towards higher, intermediate rapidities indicate increasing source velocities. (Figure 10)

To account for the apparent spectrum of velocities of the

particle-emitting sources, Westfall et al invoked the concept of the nuclear fireball (127). They assumed that in a collision between nuclei, the "participating" nucleons in the overlapping volumes of the projectile and target stick together, forming an entity called a fireball. The fireball thus moves at rapidities intermediate between target and projectile, and is assumed to be an equilibrated, non-rotating ideal gas that expands isotropically in its rest frame with a Maxwellian distribution in energy.

Because of the unequal projectile and target masses in the Ne + U collision, the kinematics of fireball production depend on the impact parameter b, and a spectrum of b-dependent fireball (source) velocities naturally arises from the model. The key assumption of a fireball system characterized only by b of the collision cannot be directly verified by these data alone. For this, equal target and projectile masses are required.

Light fragment (cluster) emission comprises a significant fraction of the total baryonic cross section (about 50% at energies 30-50 A MeV from U) (60). The cross section in velocity-space for emitting a light fragment consisting of A nucleons is roughly proportional to the A^{th} power of the cross section for emitting single nucleons of the same velocity. Models that correlate light fragments with nucleon production in velocity space in this manner are the coalescence (128, 60) and thermodynamic (129, 130) models. In the coalescence model, nucleons are assumed to form a fragment nucleus when a total of A neutrons and protons corresponding to that nucleus are emitted with vector momenta all terminating within a coalescence sphere of radius p_o. Figure 11

shows the impressive results of fitting the production cross sections to the coalescence model for d, t, ^{3}He, and ^{4}He from the reaction Ne on U at 250 and 400 A MeV, using the measured proton cross sections. The fitted values of p_o for these eight sets of data are in the range $126 \leq p_o \leq 147$ MeV/c, typical of Fermi momenta. (Figure 11)

4.2 Intermediate Rapidities

The experiment of Nagamiya et al (66) on inclusive proton spectra from the reactions 800 A MeV-^{20}Ne + $^{Pb}_{NaF}$ → p + X employs a target-centered, rotating magnetic spectrometer to obtain data at high $P_\perp$ for production angles $15^\circ \leq \theta_L \leq 145^\circ$. Proton momenta are measured in the interval $0.4 \leq p \leq 2.4$ GeV/c, the upper limit being 1.6 times the momentum/nucleon of the beam.

Figure 12 is a contour plot of the invariant cross sections $\sigma_I = Ed^2\sigma/p^2dpd\Omega$ in the $(y, P_\perp/m_pc)$-plane for proton emission from Ne on Pb. The centroids of the contours shift from $y \approx 0$ as $P_\perp/m_pc \equiv \eta_\perp$ increases. At the highest values of $\eta_\perp$ the contours approach symmetry about the average of the target and projectile rapidities $(y_P + y_T)/2$. (Figure 12)

The centroid shifts may be linear for small $\eta_\perp$. For non-relativistic, isotropically-produced protons a linear relationship, in terms of velocities, is $\beta_o = a + b\beta'$, where β_o is the velocity of the emitting source for protons with velocity $\beta' \approx \eta_\perp$ (max) in the moving frame. Stevenson et al (126) were the first to note that such a relation was a good approximation for all fragments $A \leq 16$. This permitted them to find an exponential σ_I versus momentum distribution for light fragments, independent of the fragment mass.

The reaction 800 A MeV-^{20}Ne + NaF → p + X closely approximates collisions between nuclei of equal masses. The contours of σ_I for this reaction (66) show symmetry about $\bar{y} = (y_p + y_T)/2 = 0.62$, the rapidity corresponding to 90° in the center-of-mass frame. Proton emission is not isotropic in the CM frame, but peaks forward and backward, particularly at small $\eta_\perp$. To reproduce the observed shape of the contours of σ_I requires a superposition of a spectrum of effective sources over a range of rapidities $\Delta y \approx \pm 0.2$ centered about $\bar{y}$. The elemental concept of the production of a unique fireball is not supported and, at the least, refinements of the fireball model that allows a continuum of source-velocities are necessary.

Other features of the inclusive proton spectra are:

1) The proton energy distributions at $P_\perp$ (max) for the reactions (all at 800 A MeV) C + C, Ne + NaF, C + Pb, and Ne + Pb are of the form $\sigma_I \propto \exp(-T/\tau)$, with τ in the range 68-78 MeV.

2) The target dependence of the proton yield ($\propto A_T^n$) from 800 A MeV-^{20}Ne, expressed in terms of the exponent n, approaches n = 1/3 at small angles (projectile fragmentation), and increases with angle, becoming $n \approx 1$ (or slightly greater) in the back hemisphere.

4.3 Nuclear Shock Phenomena

Searches for compression phenomena in nucleus-nucleus collisions have been carried out by Schopper and coworkers (117, 115, 131), based on studies of the angular distributions of fragments emitted from large-prong-number events in AgCl monocrystalline detectors irradiated by ^{12}C and ^{16}O projectiles, $0.25 \leqslant T \leqslant 4.2$ A GeV. Because of the

limited sensitivity of AgCl detectors, only fragments with ionization rates $I \geq 8.5\ I_{min}$ are observed. This restricts the detection of hydrogen nuclei to $T \leq 28$ A MeV, and He nuclei to $T \leq 200$ A MeV. The excess of non-evaporation He fragments, $28 \leq T \leq 200$ A MeV, in the forward hemisphere and the dependence of the peak angle of this excess on beam energy observed in the AgCl experiment have been attributed to nuclear density effects (132, 133). Other experimental searches for nuclear shock waves have not yielded positive results (74, 134, 73, 135, 113, 114, 116).

To account for the excess of fragments observed at forward angles, Schopper et al (117) have interpreted the $d\sigma/d\theta$ distributions observed in AgCl detectors as superposition of (predominantly) two spectra: a) a "background" spectrum of low-energy fragments, mainly H and He, with energies $\lesssim 28$ MeV, and b) a spectrum of He nuclei with energies $\lesssim 200$ A MeV, whose angular distribution is strongly peaked in the forward hemisphere owing to their larger mass and high energies (60, 134, 74, 116). Using the measured cross sections for $Z = 1$ and $Z = 2$ fragments (60), and the angular distribution from intranuclear cascade calculations for protons with $T \leq 250$ A MeV (122), Schopper et al were able to reproduce their observed distributions.

Based on experiments to date, it must be concluded that there is no proof for the existence of shock phenomena. It is not clear, though, that experiments performed thus far were capable of establishing the existence of such effects, in that they were predominantly single-particle inclusive measurements and/or lacked essential information on the multiplicities, energies, and isotopic identification of fragments,

including pions.

4.4 Pion Production

4.4.1 INCLUSIVE SPECTRA Rudimentary information on the angular distributions of pions produced in high-energy heavy ion collisions is available from cosmic-ray studies on shower production and from preliminary results of Bevalac experiments on the reactions 0.8 A GeV- $^{20}Ne + {}^{NaF}_{Pb} \rightarrow \pi^+ + X$ (66, 136). Known features of the angular distributions in the CM system of equal-mass particles are:

1) At high p, i.e. $\gtrsim 2\ m_\pi c$, pion emission is nearly isotropic (22, 34, 66).

2) At $P_\perp \approx m_\pi c$ (66) and CM energies $T_\pi \approx$ 100-150 MeV (136) the angular distribution shows a forward/backward peaking.

3) At CM energies 20-50 MeV, the pions are more nearly isotropic, with a possible broad peaking at $\Theta_{CM} \approx 90^\circ$ (136).

The fact that the production of pions does not depend sensitively on the structure of the projectile/target suggests independent-particle production. However, under the assumption that the cross sections are given by $d\sigma(B + T \rightarrow \pi) \approx Z_B d\sigma(p + T \rightarrow \pi) + N_B d\sigma(n + T \rightarrow \pi)$, where Z_B and N_B are the proton and neutron numbers of the projectile, it is found that the calculated cross sections agree qualitatively with experiment for $20 \lesssim T_\pi^{Lab} \lesssim 100$ MeV and $\Theta_L < 60^\circ$, but are overestimates by factors of 2 or more for $\Theta_L \geqslant 90^\circ$ (136).

The target factor index ($\sigma \propto A_T^n$) for pion production varies from $\approx$ 1/3 to 2/3 under the following conditions: a) for high pion momenta, $p_\pi > 1$ GeV/c, near $\Theta_L = 0^\circ$, n is about 1/3 (83, 137) indicative of

production in peripheral collisions; b) n increase to $\approx 1/2 - 2/3$ as p_π decreases (83). This suggests that low-momentum pions at $\theta_L \approx 0°$ are associated with more central collisions, as are pions produced at high transverse momenta, $1 < P_\perp/m_p c < 5$, which also have $n \approx 2/3$ (66).

4.4.2 MULTIPLICITIES The multiplicity distributions of pions P(n), the probability for the emission of n pions per collision, have been measured for π^- for a variety of targets and projectiles in a streamer chamber experiment (138) and for $\pi^\pm$ for ^{12}C and ^{16}O in emulsions (139) at beam energies ≈ 2 A GeV. The principal results are: a) copious production of high-multiplicity events does not occur and b) the measured P(n) can be fitted to a sum of impact-parameter-dependent Poisson distributions $P(n,b)$ that are found in a large class of dynamical models, independent of whether or not equilibrium is reached, under the condition that multipion correlations can be neglected (140).

The π^- multiplicity distribution for the reaction 1.8 A GeV-^{40}Ar + $Pb_3O_4 \rightarrow n\pi^- + X$ is shown in Figure 13a. The data are to be compared with curve 2, the calculated P(n) averaged for the Pb and O components of the target appropriate for the particular "trigger"-mode used to select events (i.e. the number of charged tracks per event > 5). Figure 13b shows the model calculations of $P(n,b)$ as a function of impact parameter for Ar and Pb. Gyulassy and Kauffmann stress that any deviation of P(n, b = 0) from a Poisson distribution would be direct evidence for unusual, coherent pion production in heavy ion collisions. (Figure 13)

4.5 Theoretical Aspects

A full description of central collisions between nuclei (or, for that matter, between nucleons) would require a quantum theory capable of dealing with infinite degrees of freedom, since both real and virtual excitations may occur. For very light nuclei a phenomenological treatment based on fits to hadron collisions is possible. For intermediate mass nuclei there may be no very good calculational scheme. If at least one and preferably both partners in a collision are very heavy, then one may hope once more to find useful models, because errors arising from crude approximations to the full theory may have little effect when averaged over almost macroscopic regions. Many different models have been compared with data on single particle inclusive reactions (142-144).

4.5.1 LONGITUDINAL MODELS One group of models might be called "longitudinal" or "one-dimensional": the collision is divided into different regions in the dimensions transverse to the beam, and communication among these regions is ignored, at least for the initial phase of the collision. The simplest of these is the fireball model, already mentioned (127). The "firestreak" model assumes sticking together and equilibration, not of the whole collection of overlapping projectile and target particles as a unit, but rather of the matter in individual narrow imaginary tubes drawn parallel to the beam direction (145). Each tube then acts as a separate emitter of product particles. In comparison to the fireball, the firestreak has the advantage that the nuclear surface diffuseness is easily accomodated, but this is not

so important for large nuclei. At moderate energies (100-400 A MeV) the fireball assumption of complete equilibration in the whole overlap region seems more reasonable. At very high energies (well above Bevalac) complete sticking together even in tubes seems unlikely. However, at energies near the top of the Bevalac range, the firestreak seems more promising, especially for large projectile and target.

A more quantum-mechanical example is the one-dimensional "row-on-row" model using Glauber theory for collisions of particles in a tube (146). This is really a way of computing and checking, rather than assuming the initial conditions of the firestreak, that is, stopping of projectile and target material in the center-of-mass frame for a given tube.

4.5.2 CLASSICAL MICROSCOPIC MODELS In these models, trajectories of individual particles are followed throughout the collision, but quantum effects are put in "by hand". The first group are cascade models of the type described in chapter 3. Here quantum mechanics is represented by the probabilistic method of determining locations and results of collisions. The simplest approach is to represent the A nucleons of a projectile by following A individual nucleon-nucleus cascades and adding the results (142). This clearly neglects all interactions of projectile nucleons among themselves, as well as most interactions of struck target nucleons with each other. A modified cascade model, in which baryon number is conserved only on the average and individual particles have probability distributions to be in various places at a given time, is computationally easier than the standard

technique when applied to nucleus-nucleus collisions (122). Full-fledged standard cascades, applicable in the moderate energy domain, are nearing completion at this writing (Z. Fraenkel & Y. Yariv, unpublished, 144).

Another kind of calculation proceeds by numerical solution of Newtonian equations of motion for nucleons interacting by two-body forces (147, 148). The forces can be made velocity-dependent in order to imitate the effect of the Pauli principle. Such models, like the cascade, are not easily extended to relativistic energies, where particle degrees of freedom proliferate.

There is even a sort of cross between the cascade and equation-of-motion approaches, in which the impact parameter of a nucleon-nucleon collision determines the scattering angle. For classical hard spheres, this gives an exact solution of the equations of motion, while for more realistic nucleon-nucleon potentials it may still be a useful approximation (149, 142). This method can be made formally relativistic, but then is no longer exact for any kind of interaction.

4.5.3 CLASSICAL MACROSCOPIC MODELS Since the proper degrees of freedom for nuclear matter at high density are not well determined from first principles, there are fundamental as well as practical arguments for describing nuclear collisions by fluid dynamics, in which the matter is treated as a fluid, always in equilibrium, with an equation of state perhaps containing phenomenological parameters to be fixed by fitting to experiment (150, 142). Two major numerical investigations were made, one using conventional relativistic nonviscous fluid dyna-

mics (150), and the other treating colliding nuclei as drops of two different fluids coupled by a frictional drag (151). At low bombarding velocities, less than the Fermi velocity $\beta_F \approx 0.2$, the one-fluid formulation makes sense, but at much higher speeds it is less reasonable, since nucleon-nucleon collisions cannot instantly share energy and momentum between projectile and target matter.

The great advantage of fluid dynamics is its power to relate experimental results to the equation of state for matter with high baryon and energy densities. The corresponding disadvantage is the assumption of local equilibrium, even in the two-fluid model. At energies much higher than Bevalac this assumption almost certainly breaks down; at least one more fluid associated with mesons must be introduced, as is done in hydrodynamic models of nucleon-nucleon collisions (152).

4.5.4 SPECIAL EFFECTS Of course, any macroscopic approach sacrifices description of singular processes such as one-step nucleon knockout, as well as of quantum correlations among emitted particles. The latter are clearly beyond any classical framework.

Spectral shapes for protons with high transverse momenta have been computed on the assumption of a single hard nucleon-nucleon scattering. Fitting to experimental data gave acceptable values for the average number of such scatterings in a collision, but could not confirm the single-step mechanism (153).

While copious data on correlations among produced particles may be expected from experiments in the near future, the main information

available so far is on the multiplicity distribution for negative pions, obtained from streamer chamber photos (138). The results have been explained in both a thermal model, where a fireball decoupling density was assumed (140), and in an approximate cascade calculation (141). The point is that minimal correlations giving a Poisson distribution of multiplicities fit well, so that at least the impact-parameter-averaged distributions carry little information.

Potentially more interesting correlations have been discussed. If some feature of the outgoing particles could signal that the collision was central with respect to both projectile and target, then single and multiple particle distributions for events with this central signal should be especially informative. It seems to us that the absence of large projectile-velocity and/or target-velocity fragments, from collisions of similar mass heavy nuclei, should be a central signal. The assumption of similar masses is important because a light projectile could be destroyed in a peripheral collision with a heavy target. On the other hand, for equal small masses the nuclei are mainly "surface", so that again destruction could occur in collisions that were far from head-on.

Two-particle momentum correlations might be used to test a single-step knockout mechanism (153), or to search for wave coherence effects in the correlation functions of identical particles, which could indicate the spatial and temporal dimensions of the effective source (154). However, such results would be interesting only if the source turned out to be surprisingly big or small.

4.5.5 APPRAISAL Comparison of model predictions for single-particle-

inclusive cross sections with each other and with experiment indicate generally better than order-of-magnitude agreement in absolute rate, and good agreement on trends with energy and angle (144), at least for bombarding energies in the range of 100-500 A MeV. This suggests that these cross sections are largely determined by geometry and conservation laws, and that the large number of degrees of freedom in the colliding system makes it possible to get the same "statistical" results with widely different approximation schemes. The rough agreement with experiment means that we have yet to find evidence for surprising or unusual phenomena in such collisions. While this might be disappointing, it suggests that existing theoretical concepts may be applicable at least to the stage of compression in central collisions of large nuclei. If so, then the crucial question becomes how, and to what degree, experimental results are affected by the nature of the evolution from that stage.

4.6 New Phases

The most dramatic suggestion for the later stages of compression is the possible formation of new phases of matter with high baryon density. Such a phase could well be more stable than ordinary nuclear matter at that density, or perhaps even more stable than matter at normal nuclear density. In the latter case, a very high barrier evidently separates ordinary matter from the new phase, since spontaneous transitions do not occur at a perceptible rate.

Proposed mechanisms leading to a new phase include the original notion of the nucleon-nucleon tensor force (4, 155); the not-so-different possibility of a very short-range attraction between nucleons (155, 156);

"quark" matter, in which these hypothetical constituents of strongly interacting particles (hadrons) would not be confined to individual nucleons, but instead could move separately throughout the nucleus (155,157); pion condensation, in which a field operator that can create and destroy pions acquires a non-zero expectation value in matter, varying from point to point in space (158); fundamental chiral symmetry, causing nucleons to become massless at sufficiently high density (159); or tensor meson exchange between nucleons (160).

More than one kind of new phase is likely to occur. A phase which is unstable with respect to ordinary matter might still produce a resonance-like energy dependence in the total cross section or in special channels, at an energy appropriate for its excitation (161).

If a new phase were absolutely stable, it probably would have much higher baryon density than ordinary nuclei. Otherwise it would be hard to understand why light nuclei do not collapse spontaneously at an appreciable rate. If a stable phase had high density, then surface effects could well make light nuclei stable in the familiar phase, while for heavy nuclei the greater barrier and greater numbers of nucleons needing to pass it would inhibit spontaneous transitions (A.K. Kerman, unpublished). In addition, a first order phase transition at relatively low density would be likely to have a great effect on neutron stars, generally agreed to be visible as pulsars, whose properties are constrained by astronomical observations (160).

Therefore, if a new stable phase can be made at all in heavy ion collisions--a proposition which has been questioned (155)--it is likely to require densities at least an order of magnitude higher than normal,

which at best would be attained with near head-on collisions of the largest nuclei at center-of-mass energies of a few A GeV, well above the Bevalac range (162). Thus, somewhat more subtle signals of new phases which are not actually stable may be the most exciting prey to pursue in the immediate future. A possible source for such a signal would be some unusual thermodynamic property of matter at high baryon density. Perhaps the most dramatic proposal up to now extends speculations about hadron structure (163) to this new domain, raising the possibility that dense matter might exhibit a "limiting temperature" $kT \approx m_\pi \approx 140$ MeV (164). That is to say, the specific heat would diverge as this temperature was approached, because more and more different states could be excited. As with other new kinds of phase, the biggest question is what effect this phenomenon would have on the particles remaining after expansion had lowered the density (164).

5. CONCLUSIONS

V.F. Weisskopf (unpublished) has compared collisions between hadrons to collisions between fine Swiss watches. His point is that the products of watch collisions are usually present before impact while the products of hadron collisions are usually formed after impact. Precisely for that reason, one should not try to learn about the structure of matter by smashing watches on each other, or even smashing atoms on each other. There are far better ways to probe these systems, so that the best to be hoped from such experiments is confirmation of insights derived in other ways. However, the case of

nuclei is quite different. High energy nuclear collisions are the only way to explore the frontier of high baryon density (165) and that alone justifies, indeed demands, further pursuit of this field.

Up to now, studies of nuclear fragmentation have revealed a rich structure, with a hierarchy of different particle energies in the rest frame of a fragmenting nucleus. Low energy (< 10 MeV "temperature") fragments are associated with peripheral interactions which "tickle" the nucleus. Slightly higher energy fragments (< 20 MeV temperature) arise from greater overlap of the colliding partners, and quite possibly are indications of the nuclear response to moderate compression and heating. In the limit of very high bombardment energies, particles with hundreds of MeV, or even GeV, energies should doubtless be considered as projectile or target fragments, just as they are in hadron collisions. Again, they should indicate the response to compression and heating.

Experiments indicate that at energies in the several hundred A MeV region head-on collisions lead to temporary pressing-together of projectile and target matter, if not full thermal equilibration. It is important to find the highest energies at which this phenomenon persists, since these will give the highest compressions and largest departures from familiar domains. In such experiments the "central" trigger coming from absence of large fragments with the velocity of the projectile, assumed equal in mass to the large target, should be a valuable tool.

In single-particle studies, searches for K^+ should give a direct

measure of strangeness production, since strangeness is not easily destroyed once created. This would give a valuable clue about the nature of compressed matter.

Looking over the results reviewed here, we see a beginning has been made in the exploration of high baryon density, a frontier which is outside traditional nuclear and particle physics. As at any frontier, there is still plenty of room for imagination and adventure, which ought to attract increasing bands of able and eager explorers.

We wish to acknowledge valuable help from many collegues, especially at the Lawrence Berkeley Laboratory. This work was supported in part by the U.S. Department of Energy and in part by the U.S. National Science Foundation. A.S.G. thanks the Nuclear Science Division of Lawrence Berkeley Laboratory and H.H.H. thanks the Institut für Kernphysik, Universitat Frankfurt for hospitality during the writing of this review.

Several related reviews have appeared recently or will appear soon. Experimental: Stock (46, 166), Schroeder (63), and Steiner (84); theoretical; Bertsch (167), Nix (144), and Gyulassy (143, 168).

Literature Cited

1. Freier, P., Lofgren, E.J., Ney, E.P., Oppenheimer, F., Bradt, H.L., and Peters, B. 1948. Phys. Rev. 74: 213-17.

2. Freier, P., Lofgren, E.J., Ney, E.P., and Oppenheimer, F. 1948. Phys. Rev. 74: 1818-27.

3. Alfvén, H. 1939. Nature 143: 435.

4. Feenberg, E. and Primakoff, H. 1946. Phys. Rev. 70: 980-81.

5. Shapiro, M.M. and Silberberg, R. 1970. Annual Review of Nuclear Science 20: 323-92.

6. Waddington, C.J. 1960. Prog. Nucl. Phys. 8: 1-45.

7. Powell, C.F., Fowler, P.H., and Perkins, D.H. 1959. The Study of Elementary Particles by the Photographic Method. London: Pergamon. 669 pp.

8. Bradt, H.L. and Peters, B. 1948. Phys. Rev. 74: 1828-37.

9. Bradt, H.L. and Peters, B. 1949. Phys. Rev. 75: 1779-80.

10. Bradt, H.L. and Peters, B. 1950. Phys. Rev. 77: 54-70.

11. Bradt, H.L. and Peters, B. 1950. Phys. Rev. 80: 943-53.

12. Kaplon, M.F., Peters, B., Reynolds, H.L., and Ritson, D.M. 1952. Phys. Rev. 85: 295-309.

13. Cleghorn, T.F. 1967. Thesis on The Energy Dependence of the Fragmentation Parameters and Interaction Mean Free Paths in Nuclear Emulsion for Heavy Cosmic Ray Nuclei, Report No. CR-104. University of Minnesota, 75 pp.

14. Cleghorn, T.F., Freier, P.S., and Waddington, C.J. 1968. Canadian J. Phys. 46: 572-77.

15. Lohrmann, E. and Teucher, M.W. 1959. Phys. Rev. 115: 636-42.

16. Eisenberg, Y. 1954. Phys. Rev. 96: 1378-82.

17. Bowman, J.D., Swiatecki, W.J., and Tsang, C.F. 1973. Lawrence Berkeley Laboratory Report LBL-2908. 22 pp.

18. Alexander, G. and Yekutieli, G. 1961. Nuovo Cimento 19: 103-17; Alexander, G., Avidan, J., Avni, A., and Yekutieli, G. 1961. Nuovo Cimento 20: 648-61.

19. Aizu, H., Fujimoto, Y., Hasegawa, S., Koshiba, M., Mito, I., Nishimura, J., and Yokoli, K. 1961. Prog. Theo. Phys. Suppl. 16: 54-168.

20. Fernbach, S., Serber, R., and Taylor, T.B. 1949. Phys. Rev. 75: 1352-55.

21. Glauber, R.J. 1959. Lectures in Theoretical Physics, edited by W.B. Britton et al, Wiley-Interscience, New York, Vol. 1, p. 315-414.

22. Jain, P.L., Lohrmann, E., and Teucher, M.W. 1959. Phys. Rev. 115: 643-54.

23. Tsuzuki, Y. 1961. Jour. Phys. Soc. of Japan 16: 2131-39.

24. Rybicki, K. 1963. Nuovo Cimento 28: 1437-54.

25. Abraham, F., Gierula, J., Levi-Setti, R., Rybicki, K., and Tsao, C.H. 1967. Phys. Rev. 159: 1110-23.

26. Andersson, B., Otterlund, I., and Kristiansson, K. 1966. Arkiv Fysik 31: 527-48.

27. Otterlund, I. and Andersson, B. 1967. Arkiv Fysik 35: 133-47.

28. Otterlund, I. 1968. Arkiv Fysik 38: 467-87.

29. Otterlund, I. and Resmanm R. 1969. Arkiv Fysik 39: 265-93.

30. Resman, R. and Otterlund, I. 1971. Phys. Scripta 4: 183-9.

31. Kullberg, R., Otterlund, I., and Resman, R. 1972. Phys. Scripta 5: 5-12.

32. Kullberg, R. and Otterlund, I. 1973. Z. Physik 259: 245-62.

33. Jakobsson, B., Kullberg, R., and Otterlund, I. 1974. Z. Physik 268: 1-9.

34. Jakobsson, B., Kullberg, R., and Otterlund, I. 1975. Z. Physik A 272: 159-68.

35. Skeggestad, P. and Sörensen, S.O. 1959. Phys. Rev. 113: 1115-24.

36. Hyde, E.K., Butler, G.W., and Poskanzer, A.M. 1971. Phys. Rev. C 4: 1759-78.

37. Gagarin, Yu.F., Ivanova, N.S., and Kulikov, V.N. 1970. Sov. J. Nucl. Phys. 11: 698-703.

38. Gottstein, K. 1954. Phil. Mag. 45: 347-59.

39. Cester, R., DeBenedetti, A., Garelli, C.M., Quassiati, B., Tallone, L., and Vigone, M. 1958. Nuovo Cimento 7: 371-99.

40. Particle Data Group. 1976. Rev. Mod. Phys. No. 2, Part II 48: S1-245.

41. Grunder, H.A. and Selph, F.B. 1977. Heavy Ion Accelerators, Annual Review of Nuclear Science. In press.

42. Goulding, F.S. and Harvey, B.G. 1975. Identification of Nuclear Particles, Annual Review of Nuclear Science 25: 167-240.

43. Price, P.B. and Fleischer, R.L. 1971. Annual Review of Nuclear Science 21: 295-330.

44. Fleischer, R.L., Price, P.B., and Walker, R.M. 1975. Nuclear Tracks in Solids, Univ. of California Press. 605 pp.

45. Barkas, W.H. 1963. Nuclear Research Emulsions, New York:

Academic Press. 518 pp.

46. Stock, R. Heavy Ion Collisions, North Holland, Vol. 1, R. Bock, ed. In press.

47. Rosen, L. 1971. IEEE Trans. on Nucl. Sci. NS-18, No. 3: 29-35.

48. White, M.G. 1971. IEEE Trans. on Nucl. Sci. 174: 1121-23.

49. Ghiorso, A., Grunder, H., Hartsough, W., Lambertson, G., Lofgren, E., Lou, K., Main, R., Mobley, R., Morgado, R., Salsig, W., and Selph, F. 1973. IEEE Trans. on Nucl. Sci. NS-20, No. 3: 155-58.

50. White, M.G., Isaila, M., Prelec, K., and Allen, H.L. 1971. Science 174: 1121-23; Grunder, H.A., Hartsough, W.D., and Lofgren, E.J. 1971. Science 174: 1128-29.

51. Farley, F.J.M. 1970. Speculations on Nucleus-Nucleus Collisions with the ISR, CERN NP Internal Report 70-26, 6 pp.

52. Baldin, A.M. 1977. Sov. J. of Particles and Nuclei 8: 430-77.

53. GANIL Study Group. 1975. IEEE Trans. on Nucl. Sci. NS-22, No. 3: 1651-54.

54. Study Group of Numatron Project. 1977. Proposal for Numatron, Institute for Nuclear Study, University of Tokyo, 354 pp.

55. Baldin, A.M. 1975. Proc. High-Energy Physics and Nuclear Structure-1975. American Institute of Physics, New York. pp. 621-41.

56. Study Report. 1977. Gesellschaft für Schwerionenforschung. MBH, GSI-P-2-77. 39 pp.

57. Nuclear Chemistry Annual Report. 1972. Lawrence Berkeley Laboratory

LBL-1666.

58. Grunder, H.A. 1975. IEEE Trans. on Nucl. Sci. NS-22, No. 3: 1621-25.

59. High Intensity Uranium Beams from the SuperHILAC and the Bevatron. Proposal-32.

60. Gosset, J., Gutbrod, H.H., Meyer, W.G., Poskanzer, A.M., Sandoval, A., Stock, R., and Westfall, G.D. 1977. Phys. Rev. C 16: 629-57.

61. Greiner, D.E., Lindstrom, P.J., Bieser, F.S., and Heckman, H.H. 1974. Nucl. Inst. and Meth. 116: 21-24.

62. Anderson, L. 1977. Thesis, Univ. of California, Berkeley, LBL-6769, 133 pp.

63. Schroeder, L.S. 1977. Acta Phys. Polonica B8: 355-87.

64. Childs, C.B. and Slifkin, L. 1963. Rev. Sci. Inst. 34: 101-4.

65. Haase, G., Schopper, E., and Granzer, F. 1973. Phot. Sci. and Eng. 17: 409-12.

66. Nagamiya, S., Tanihata, I., Schnetzer, S., Anderson, L., Brückner, W., Chamberlain, O., Shapiro, G., and Steiner, H. 1977. Proc. Int. Conf. on Nucl. Structure, Tokyo, Japan, Sept. 5-10. Also Lawrence Berkeley Laboratory Report LBL-6770, 25 pp.

67. Benecke, J., Chou, T.T., Yang, C.N., and Yen, E. 1969. Phys. Rev. 188: 2159-69.

68. Feynman, R.P. 1969. Phys. Rev. Lett. 23: 1415-17.

69. Gell-Mann, M. 1962. Phvs. Rev. Lett. 8: 263-64; Gribov, V.N. and Pomeranchuk, I.Ya. 1962. Phys. Rev. Lett. 8: 343-45.

70. Feshbach, H. and Huang, K. 1973. Phys. Letters 47B: 300-2.

71. Jaros, J. 1975. Thesis, Lawrence Berkeley Laboratory Report LBL-3849. 116 pp.

72. Heckman, H.H., Greiner, D.E., Lindstrom, P.J., and Shwe, H. 1978. Phys. Rev. C 17. In press.

73. Chernov, G.M., Gulamov, K.G., Gulyamov, U.G., Nasyrov, S.Z., and Svechnikova, L.N. 1977. Nucl. Phys. A 280: 478-90.

74. Jakobsson, B. and Kullberg, R. 1976. Physica Scripta 13: 327-38.

75. Judek, B. 1975. Proc. 14th Int. Conf. on Cosmic Rays, München. pp. 2342-47.

76. Kullberg, R., Kristiansson, K., Lindkvist, B., and Otterlund, I. 1977. Nucl. Phys. A280: 491-97.

77. Cheshire, D.L., Huggett, R.W., Johnsson, D.P., Jones, W.V., Rountree, S.P., Verma, S.D., Schmidt, W.K.H., , R.J., Bowen, T., and Krider, E.P. 1974. Phys. Rev. D 10: 25-31.

78. Lindstrom, P.J., Greiner, D.E., Heckman, H.H., Cork, B., and Bieser, F.S. 1974. Proc. 14th Int. Conf. on Cosmic Rays, München. pp. 2315-18.

79. Barshay, S., Dover, C.B., and Vary, J.P. 1975. Phys. Rev. C 11: 360-69.

80. Karol, P.J. 1975. Phys. Rev. C 11: 1203-9.

81. Heckman, H.H., Greiner, D.E., Lindstrom, P.J., and Bieser, F.S. 1972. Phys. Rev. Lett. 28: 926-29.

82. Lindstrom, P.J., Greiner, D.E., Heckman, H.H., Cork, B., and Bieser, F.S. 1975. Lawrence Berkeley Laboratory Report LBL-3650. 10 pp.

83. Papp, J., Jaros, J., Schroeder, L., Staples, J., Steiner, H., Wagner, A., and Wiss, J. 1975. Phys. Rev. Lett. 10: 601-4.

84. Steiner, H.L. 1977. Proc. of VII Int. Conf. on High-Energy Physics and Nuclear Structure, Zurich, 29 Aug-2 Sept. M. Locher, ed. pp. 261-286.

85. Raisbeck, G.M. and Yiou, F. 1975. Phys. Rev. Lett. 35: 155-59.

86. Heckman, H.H. and Lindstrom, P.J. 1976. Phys. Rev. Lett. 37: 56-9.

87. Greiner, D.E., Lindstrom, P.J., Heckman, H.H., Cork, B., and Bieser, F.S. 1975. Phys. Rev. Lett. 35: 152-55.

88. Lepore, J.V. and Riddell, R.J. Jr. 1974. Lawrence Berkeley Laboratory Report LBL-3086. 24 pp.

89. Goldhaber, A.S. 1974. Phys. Letters 53B: 306-8.

90. Masuda, N. and Uchiyama, F. 1975. Lawrence Berkeley Laboratory Report LBL-4263. 24 pp.

91. Bizard, G., LeBrun, C., Berger, J., Duflo, J., Goldzahl, L., Plouin, F., Oostens, J., Van Den Bossche, M., Vu Hai, L., Fabbri, F.L., Picozza, P., and Satta, L. 1977. Nucl. Phys. A 285: 461-68.

92. Schmidt, I.A. and Blankenbecler, R. 1977. Phys. Rev. D 15: 3321-31.

93. Frankel, S., Frati, W., Van Dyck, O., Werbeck, R., and Highland, V. 1976. Phys. Rev. Lett. 36: 642-45.

94. Frankel, S. 1977. Phys. Rev. Lett. 38: 1338-41.

95. Dar, A. 1976. Proc. of the Meeting on Nucl. Prod. at Very High Energies, S.A. Azimov, ed. Trieste.

96. Burov, V.V., Lukyanov, V.K., and Titov, A.I. 1977. Phys. Letters 67B: 46-48.

97. Fujita, T. 1977. Phys. Rev. Lett. 39: 174-76.

98. Buenerd, M., Gelbke, C.K., Harvey, B.G., Hendrie, D.L., Mahoney, J., Menchaca-Rocha, A., Olmer, C., and Scott, D.K. 1976. Phys. Rev. Lett. 37: 1191-94.

99. Gelbke, C.K., Buenerd, M., Hendrie, D.L., Mahoney, J., Mermaz, M.C., Olmer, C., and Scott, D.K. 1976. Phys. Rev. Lett. 37: 1191-4.

100. Gelbke, C.K., Olmer, C., Buenerd, M., Hendrie, D.L., Mahoney, J., Mermaz, M.C., and Scott, D.K. 1977. Lawrence Berkeley Laboratory Report LBL-5826. 116 pp.

101. Gelbke, C.K., Scott, D.K., Bini, M., Hendrie, D.L., Laville, J.L., Mahoney, J., Mermaz, M.C., and Olmer, C. 1977. Phys. Letters 70 B: 415-17.

102. Westfall, G.D., Sextro, R.G., Poskanzer, A.M., Zebelman, A.M., Butler, G.W., and Hyde, E.K. 1978. Phys. Rev. C. In press.

103. Korteling, R.G. and Hyde, E.K. 1964. Phys. Rev. B 136: 425-36.

104. Karol, P.J. 1974. Phys. Rev. C 10: 150-5.

105. Cumming, J.B., Stoenner, R.W., and Haustein, P.E. 1976. Phys. Rev. C 14: 1554-63.

106. Cumming, J.B., Haustein, P.E., Stoenner, R.W., Mausner, L., and Naumann, R.A. 1974. Phys. Rev. C 10: 739-55.

107. Cumming, J.B., Haustein, P.E., Ruth, T.J., and Virtes, G.J. 1977. Brookhaven National Laboratory Report BNL-25378. 38 pp.

108. Rudy, C.R. and Porile, N.T. 1975. Phys. Letters 59 B: 240-3.

109. Loveland, W., Otto, R.J., Morrissey, D.J., and Seaborg, G.T. 1977. Phys. Letters 69 B: 284-86.

110. Loveland, W., Otto, R.J., Morrissey, D.J., and Seaborg, G.T. 1977. Phys. Rev. Lett. 39: 320-2.

111. Katcoff, S. and Hudis, J. 1976. Phys. Rev. C 14: 628-34.

112. Zebelman, A.M., Poskanzer, A.M., Bowman, J.D., Sextro, R.G., and Viola, V.E. Jr. 1975. Phys. Rev. C 11: 1280-86.

113. Jakobsson, B., Kullberg, R., and Otterlund, I. 1977. Nucl. Phys. A 276: 523-32.

114. Heckman, H.H., Crawford, H.J., Greiner, D.E., Lindstrom, P.J., and Wilson, L.W. 1978. Phys. Rev. C 17. In press.

115. Baumgardt, H.G., Schott, J.U., Sakamoto, Y., Schopper, E., Stöcker, H., Hofmann, J., Scheid, W., and Greiner, W. 1975. Z. Phys. A 237: 359-71.

116. Heckman, H.H., Crawford, H.J., Greiner, D.E., Lindstrom, P.J., and Wilson, L.W. 1977. Proc. of the Meeting on Heavy Ion Collisions, Fall Creek Falls, Tennessee, June 13-17. Oak Ridge National Laboratory Report CONF-770602. pp. 411-432.

117. Schopper, E., Baumgardt, H.G., and Obst, E. 1977. Proc. of the Meeting on Heavy Ion Collisions, Fall Creek Falls, Tennessee, June 13-17. Oak Ridge National Laboratory Report CONF-770602. pp. 398-410.

118. Masuda, N. and Uchiyama, F. 1977. Phys. Rev. C 15: 1598-600.

119. Glauber, R.J. and Matthiae, G. 1970. Nucl. Phys. B21: 135-57; Blieden, H.R., Finocchiaro, G., Goldhaber, A.S., Grannis, P.D.,

Green, D., Hietarinta, J., Hochman, D., Kephart, R., Kirz, J., Lee, Y.Y., Nef, C., Thun, R., Faissler, W., and Tang, Y.W. 1975. Phys. Rev. D 11: 14-28.

120. Franco, V. and Varma, G.K. 1977. Phys. Rev. C 15: 1375-78; Franco, V. and Tekou, A. 1977. Phys. Rev. C 16: 658-64; Franco, V. and Nutt, W.T. 1977. Nucl. Phys. In press.

121. Bertini, H.W. Santoro, R.T., and Hermann, O.W. 1976. Phys. Rev. C 14: 590-95.

122. Smith, R.K. and Danos, M. 1977. Proc. on the Meeting on Heavy Ion Collisions, Fall Creek Falls, Tennessee, June 13-17, Oak Ridge National Laboratory Report CONF-770602. pp. 363-80.

123. Hüfner, J., Schäfer, K., and Schürmann, B. 1975. Phys. Rev. C 12: 1888-98; Abdul-Magd, A. and Hüfner, J. 1976. Z. Phys. A 277: 379-84; Abdul-Magd, A., Hüfner, J., and Schürmann, B. 1976. Phys. Letters 60B: 327-30; Celenza, L.S., Hüfner, J., and Sander, C. 1977. Nucl. Phys. A 276: 509-22.

124. Lukyanov, V.K. and Titov, A.I. 1975. Phys. Letters 57B: 10-12.

125. Crawford, H.J., Price, P.B., Stevenson, J., and Wilson, L.W. 1975. Phys. Rev. Lett. 34: 329-31.

126. Stevenson, J., Price, P.B., and Frankel, K. 1977. Phys. Rev. Lett. 38: 1125-29.

127. Westfall, G.D., Gosset, J., Johansen, P.J., Poskanzer, A.M., Meyer, W.G., Gutbrod, H.H., Sandoval, A., and Stock, R. 1976. Phys. Rev. Lett. 37: 1202-5.

128. Gutbrod, H.H., Sandoval, A., Johansen, P.J., Poskanzer, A.M.,

Gosset, J., Meyer, W.G., Westfall, G.D., and Stock, R. 1976. Phys. Rev. Lett. 37: 667-69.

129. Mekjian, A. 1977. Phys. Rev. Lett. 38: 640-43; Mekjian, A., Bond, R., Johansen, P.J., Koonin, S.E., and Garpman, S.I.A. 1977. Phys. Letters 71B: 43-47.

130. Alard, J.P., Baldit, A., Brun, R., Costilhes, J.P., Dhermain, J., Fargeix, J., Fraysse, L., Pellet, J., Roche, G., and Tamain, J.C. 1975. Nuovo Cimento: 30: 320-44.

131. Baumgardt, H.G., Schopper, E., Schott, J.U., Kocherov, N.P., Vorohov, A.V., Issinsky, I.D., and Markov, L.G. 1976. Proc. IV Int. Workshop on Gross Properties of Nuclei, Hirschegg, Austria, AED Conf. 76-015-000. pp. 105-10.

132. Hofmann, J., Stöcker, H., Gyulassy, M., Scheid, W., Greiner, W., Baumgardt, H.G., Schott, J.U., and Schopper, E. 1976. Proc. Int. Conf. on Selected Topics in Nuclear Structure, Dubna, USSR, D-9920.

133. Hofmann, J., Stöcker, H., Heinz, U., Scheid, W., and Greiner, W. 1976. Phys. Rev. Lett. 36: 88-91; Stöcker, H. 1977. Proc. of Int. Symp. on Nucl. Collisions and Their Microscopic Description, Bled, Yugoslavia, 26 Sept-1 Oct. FIZIKA 9: Suppl. 4, pp. 671-706.

134. Poskanzer, A.M., Sextro, R.G., Zebelman, A.M., Gutbrod, H.H., Sandoval, A., and Stock, R. 1975. Phys. Rev. Lett. 35: 1701-4.

135. Basova, E.S., Bondarenko, A.I., Gulamov, K.G., Gulyamov, U.G., Nasyrov, Sh.Z., Svechnikova, L.N., and Chernov, G.M. 1976. JETP Lett. 24: 229-32.

136. Nakai, K., Chiba, J., Tanihata, I., Nagamiya, S., Bowman, H., Ioannou, J., and Rasmussen, J.O. 1977. Proc. Int. Conf. on Nuclear Structure, Tokyo, Japan, Sept. 5-10. In press.

137. Schimmerling, W., Vosburgh, K.G., and Koepke, K. 1974. Phys. Rev. Lett. 33: 1170-73.

138. Fung, S.Y., Gorn, W., Kiernan, G.P., Liu, F.F., Lu, J.J., Oh, Y.T., Ozawa, J., Poe, R.T., Schroeder, L., and Steiner, H. 1978. Phys. Rev. Lett. 40: 292-5.

139. Jakobsson, B., Kullberg, R., Otterlund, I., Ruiz, A., Bolta, J.M., and Higón, E. 1977. University of Lund, Department of Cosmic and Subatomic Physics, Report LUIP-7708. 26 pp.

140. Gyulassy, M. and Kauffman, S.K. 1978. Phys. Rev. Lett. 40: 298-302.

141. Vary, J.P. 1978. Phys. Rev. Lett. 40: 295-98.

142. Amsden, A.A., Ginocchio, J.N., Harlow, F.H., Nix, J.R., Danos, M., Halbert, E.C., and Smith, R.K. Jr. 1977. Phys. Rev. Lett. 38: 1055-58.

143. Gyulassy, M. 1977. Proc. of Int. Symp. on Nucl. Collisions and their Microscopic Description, Bled, Yugoslavia, 26 Sept-1 Oct. FIZIKA 9: Suppl. 4, pp. 623-70.

144. Nix, J.R. 1978. Prog. in Part. and Nucl. Phys. 1, D.H. Wilkinson, ed. In press.

145. Myers, W.D. 1978. Nucl. Phys. A296: 177-88.

146. Hufner, J. and Knoll, J. 1977. Nucl. Phys. A290: 460-92.

147. Bodmer, A.R. and Panos, C.N. 1977. Phys. Rev. C 15: 1342-58;

Bodmer, A.R. 1977. Proc. of Meeting on Heavy Ion Collisions, Fall Creek Falls, Tennessee, June 13-17, Oak Ridge National Laboratory Report CONF-770602. pp. 309-62.

148. Wilets, L., Henley, E.M., Kraft, M., and MacKellar, A.D. 1977. Nucl. Phys. A282: 341-50; Wilets, L., MacKellar, A.D., and Rinker, G.A. Jr. 1976. Proc. IV Int. Workshop on Gross Properties of Nuclei, Hirschegg, Austria, Institut für Kernphysik Technische Hoshschule, Darmstadt Report AED-Conf-76-015-000. pp. 111-14; Wilets, L., Yariv, Y., and Chestnut, R. 1977. University of Washington Report RLO-1388-744. 11 pp.

149. Bondorf, J.P., Feldmeier, H.T., Garpman, S.I.A., and Halbert, E.C. 1976. Phys. Letters 65B: 217-20.

150. Amsden, A.A., Bertsch, G.F., Harlow, F.H., and Nix, J.R. 1975. Phys. Rev. Lett. 35: 905-8; Amsden, A.A., Harlow, F.H., and Nix, J.R. 1977. Phys. Rev. C 15: 2059-71.

151. Amsden, A.A., Goldhaber, A.S., Harlow, F.H., and Nix, J.R. 1977. Los Alamos Scientific Laboratory Report LA-UR-77-2691.

152. Landau, L.D. 1953. Isv. Akad. Nauk, SSRR, Ser. Fiz. 17: 51; Cooper, F. 1975. Particles and Fields-1974, American Institute of Physics Conference Proceedings No. 23, C.E. Carlson, ed. American Institute of Physics, New York. pp. 499.

153. Koonin, S.E. 1977. Phys. Rev. Lett. 39: 680-84.

154. Goldhaber, G., Goldhaber, S., Lee, W., and Pais, A. 1960. Phys. Rev. 120: 300-12; Kopylov, G.I. 1974. Phys. Letters 50B: 472-74; Koonin, S.E. 1977. Phys. Letters 70B: 43-47.

155. Bodmer, A.R. 1971. Phys. Rev. D 4: 1601-6; The Nuclear Many-

Body Problem, F. Calogero and C. Ciofi Degli Atti, ed., Editrice Compositori, Bologna. 1971. 2: 505-34.

156. Ne'eman, Y. 1968. Proc. Fifth Conf. on Symmetry Principles at High Energy, W.A. Benjamin, New York. pp. 149-51; Proc. Int. Astron. Union Symp. No. 53 on Physics of Dense Matter. 1974. D. Reidel, publ. pp. 111.

157. Collins, J.C. and Perry, M.J. 1975. Phys. Rev. Lett. 34: 1353-56.

158. Migdal, A.B. 1971. Zh. Eksp. Teor. Fiz. 61: 2209; Migdal, A.B. 1972. Sov. Phys. JETP 34: 1184; Sawyer, R.F. 1972. Phys. Rev. Lett. 29: 382-85; Scalapino, D.J. 1972. Phys. Rev. Lett. 29: 386-88; Brown, G.E. and Weise, W. 1976. Phys. Rep. 27C: 1-34; Ruck, V., Gyulassy, M., and Greiner, W. 1976. Z. Phys. A277: 391-94.

159. Lee, T.D. and Wick, G.C. 1974. Phys. Rev. D 9: 2291-303; Lee, T.D. 1975. Rev. Mod. Phys. 4: 267-75; Lee, T.D., Mesons in Nuclei, M. Rho and D.H. Wilkinson, eds. In press.

160. Canuto, V., Datta, B., and Kalman, G. 1978. Ap. J. In press.

161. Chapline, G.F. and Kerman, G. 1977. Lawrence Livermore Laboratory Report. 12 pp.

162. Goldhaber, A.S. 1977. Lawrence Berkeley Laboratory Report LBL-6595. 8 pp.

163. Hagedorn, R. 1973. Cargése Lectures in Physics, E. Schatzman, ed. Gordon and Breach, New York. Vol. 6, pp. 643-716.

164. Glendenning, N.K. and Karant, Y.J. 1977. Phys. Rev. Lett. 40: 374-77.

165. Chapline, G.F., Johnson, M.H., Teller, E., and Weiss, M.S. 1973. Phys. Rev. D 8: 4302-8.

166. Stock, R. 1978. Phys. Rep. In press.

167. Bertsch, G.F. 1977. Proc. Summer School on Heavy Ions and Mesons in Nuclear Physics, Les Houches, France. In press.

168. Gyulassy, M. 1978. Phys. Rep. In press.

TABLE 1. Heavy Ion Facilities, $Z \geqslant 2$ and $T/A \geqslant 0.1$ GeV.

Location	Accelerator	Ion	Energy/A (GeV)	Intensity (Extracted, ppp)	Pulse rate
Saclay	Saturne	^{4}He	$\leqslant 1.2$	2×10^{10} ppp	$15/\text{min}^{-1}$
Dubna (JINR) (52)	Synchrophasotron	^{4}He	$\leqslant 5.0$		
		^{12}C	$\leqslant 5.0$		
		^{20}Ne	$\leqslant 5.0$		
Berkeley (LBL)	Berkeley*	^{6}Li	0.1-2.1		$10/\text{min}^{-1}$, $15/\text{min}^{-1}$ at $T/A \leqslant 0.4$ GeV
		^{12}C	"	2×10^{9}	" "
		^{14}N	"	"	" "
		^{16}O	"	"	" "
		^{20}Ne	"	8×10^{8}	" "
		^{40}Ar	1.8	5×10^{8}	" "
		^{56}Fe	1.9	$1\text{-}2 \times 10^{5}$	" "
	Berkeley†	^{4}He	0.1-2.1	$1\text{-}2 \times 10^{10}$	
		^{12}C	"	1×10^{8}	

* SuperHILAC injector: $T/A = 8.5$ MeV

** By end of 1978, Saturne will accelerate $Z/A = 1/2$ nuclei through ^{20}Ne; $T/A = 0.10\text{-}1.1$ GeV

† Local linear accelerator for injector: $T/A = 5$ MeV

Figure Captions

Figure 1 Interaction of an ^{40}Ar projectile, T = 1.8 A GeV, with a Ag(Br) nucleus in Ilford G.5 emulsion that shows characteristics of both projectile and target fragmentation.

Figure 2 Interaction of an ^{40}Ar projectile, T = 1.8 A GeV, with a Pb nucleus (Pb_3O_4 target) in the LBL streamer chamber leading to the catastrophic destruction of target and projectile nuclei. Negative particles have counter-clockwise trajectories in the magnetic field of the chamber (Courtesy of UC Riverside/LBL collaboration).

Figure 3 Angular distributions of shower particles from the interactions of cosmic-ray heavy ions, $3 \leqslant Z \leqslant 26$ and $T \geqslant 1.7$ A GeV, with emulsion nuclei, a) $0^\circ \leqslant \theta_L \leqslant 80^\circ$ and b) $0^\circ \leqslant \theta_L \leqslant 12^\circ$. Curves are calculated distributions of pions for projectile energies 5 to 20 A GeV (26).

Figure 4 Measured total cross sections $\sigma_{TOT}(AA)$ vs. A compared with predictions by Glauber theory and from factorization (71).

Figure 5 Rigidity spectrum of carbon isotopes produced by the fragmentation of ^{16}O projectiles at 2.1 A GeV. Arrows indicate the rigidities for each isotope evaluated at beam velocity (87).

Figure 6 The projectile frame longitudinal momentum distribution for ^{10}Be fragments from 2.1 A GeV-^{12}C on a Be target (87).

Figure 7 Transverse momentum distributions of beam-velocity protons produced in the reaction α + C for three different beam momenta (62).

Figure 8 Invariant cross sections for π^- production at $\theta_L = 2.5°$ a) incident protons, b) incident deuterons and alphas, on ^{12}C (83). Curves are from Ref. (92).

Figure 9 Charge dispersion curves for products in the mass range $37 \leqslant A \leqslant 61$ from the spallation of copper by 3.9-GeV ^{14}N ions and by protons. The lower curves and filled points are for protons; the upper curves and open points are for ^{14}N. The curves are displaced vertically by a factor of 10 for display purposes (106).

Figure 10 Contours of constant invariant cross section in the $(y, P_\perp)$ plane for ^3He fragments from ^{20}Ne on U at different bombarding energies (60).

Figure 11 Double differential cross sections for hydrogen and helium isotopes from ^{20}Ne on U compared with calculations (curves) using the coalescence formalism (60).

Figure 12 Contours of constant invariant cross section, σ_I, in the $(y, \eta_\perp)$ plane for the reaction 0.8 A GeV-Ne + Pb → p + X (66).

Figure 13 π^- multiplicity distributions for Ar + Pb_3O_4 at 1.8 A GeV. a) Data are from Ref (138). Curves (1) and (2) are from Ref. (140); (1)--no impact parameter b cutoff, (2)--with $b_{max}(Pb) = 9.6$ fm, $b_{max}(O) = 5.0$ fm. Dashed curves give contributions to (2) from Pb and O targets. Points denoted by ∇ are from Ref. (141). b) Calculated distributions plotted as a function of impact parameter b (140).

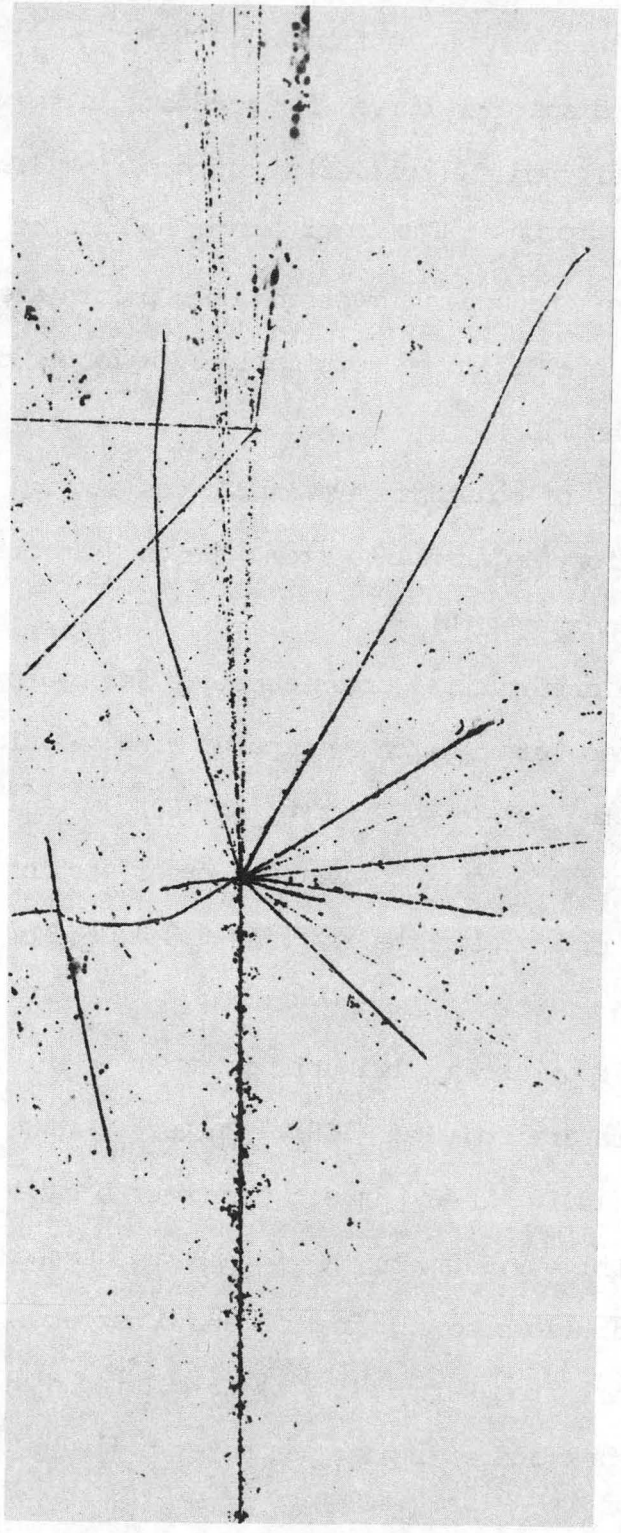

XBB 771-32

Figure 1

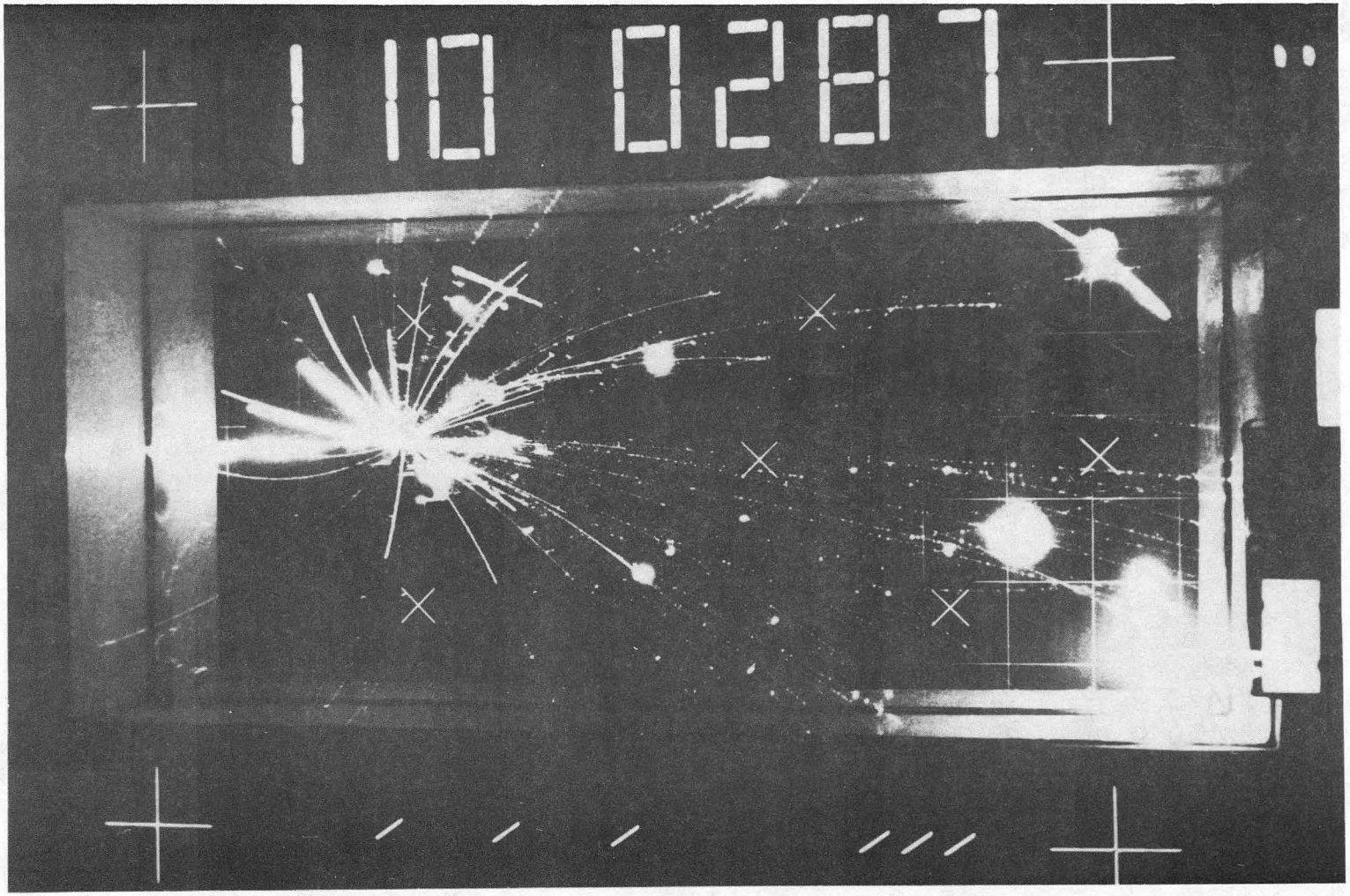

XBB 751-8445

Figure 2

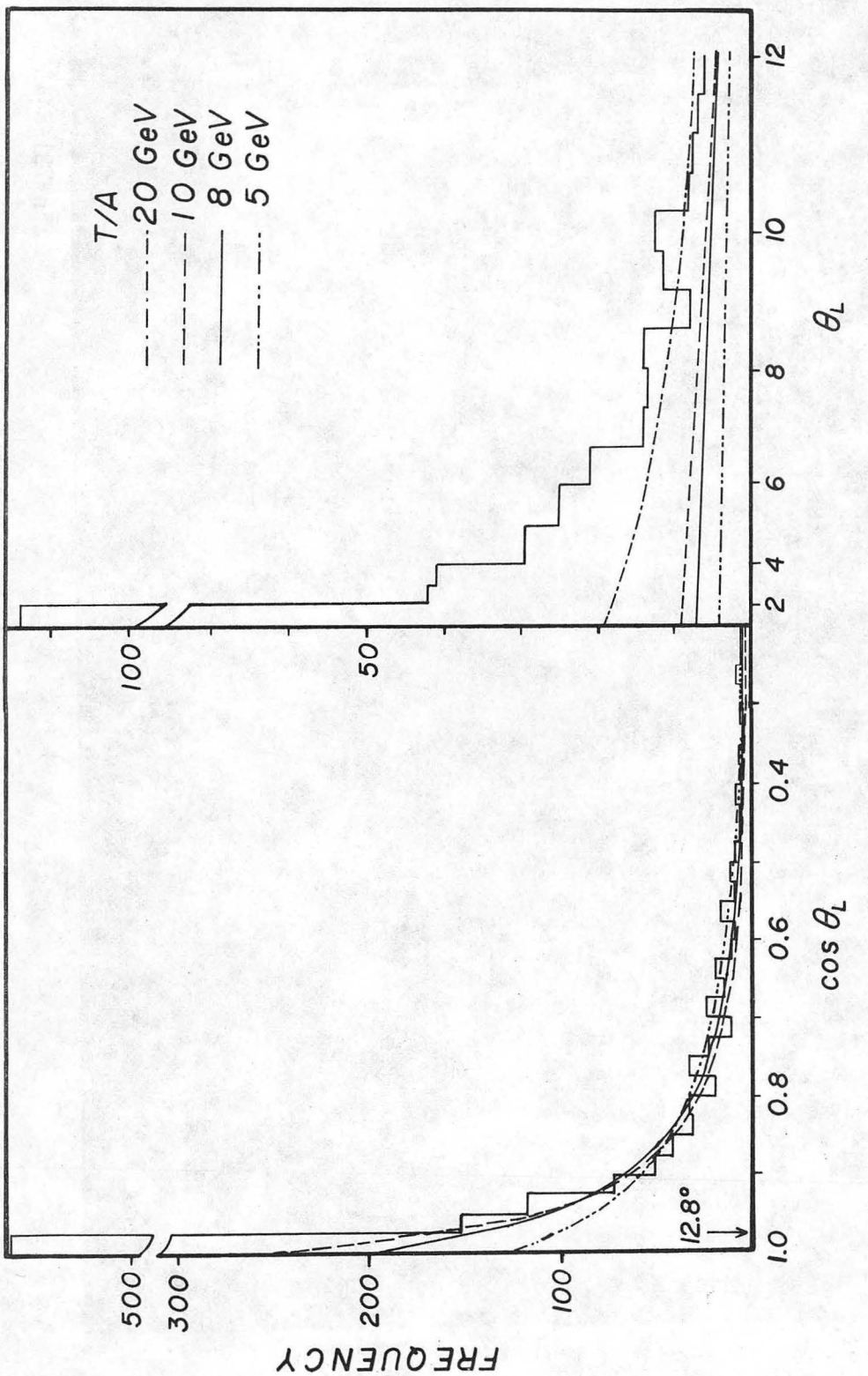

XBL 781-6750

Figure 3

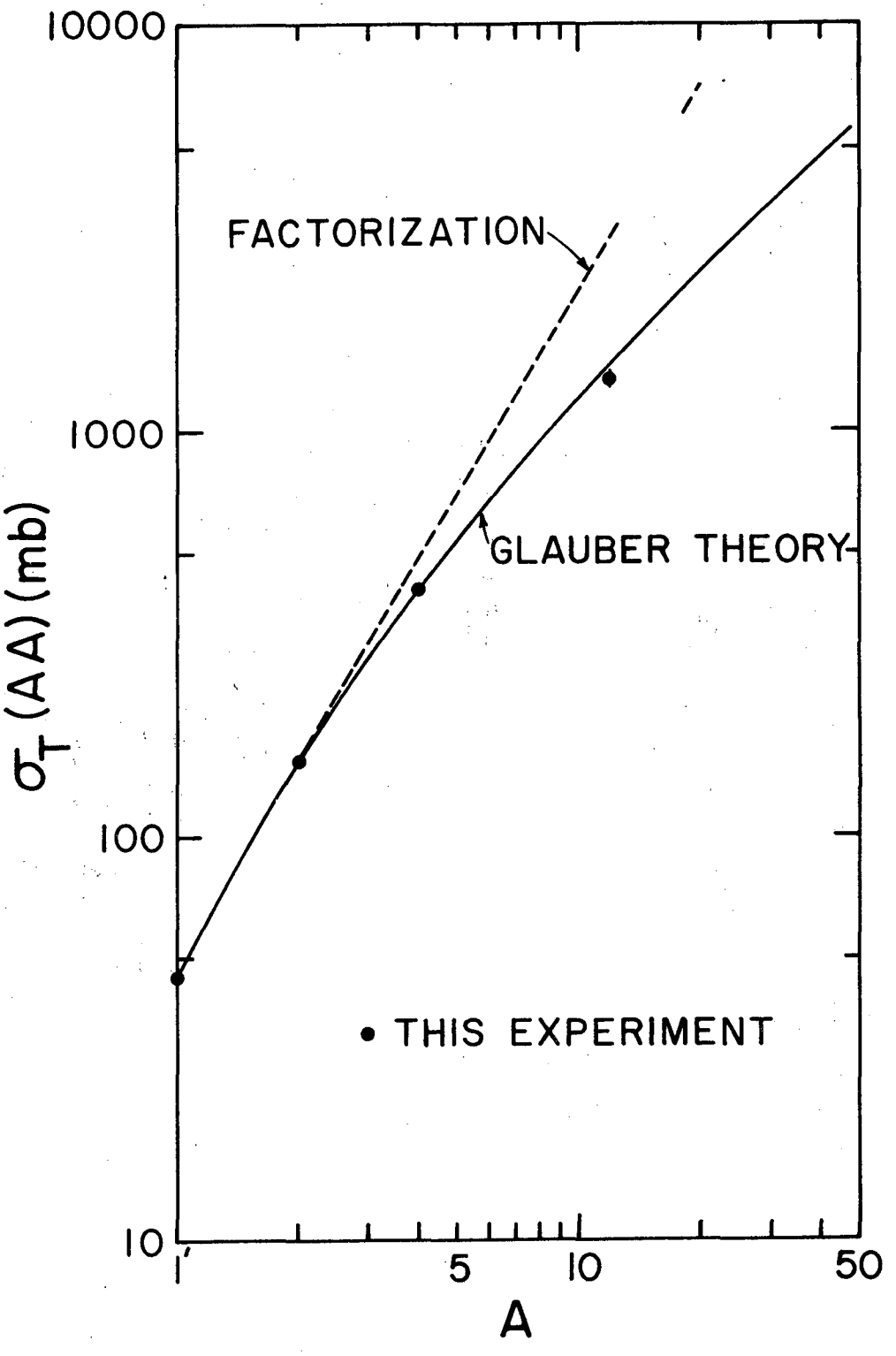

XBL 7511-9045

Figure 4

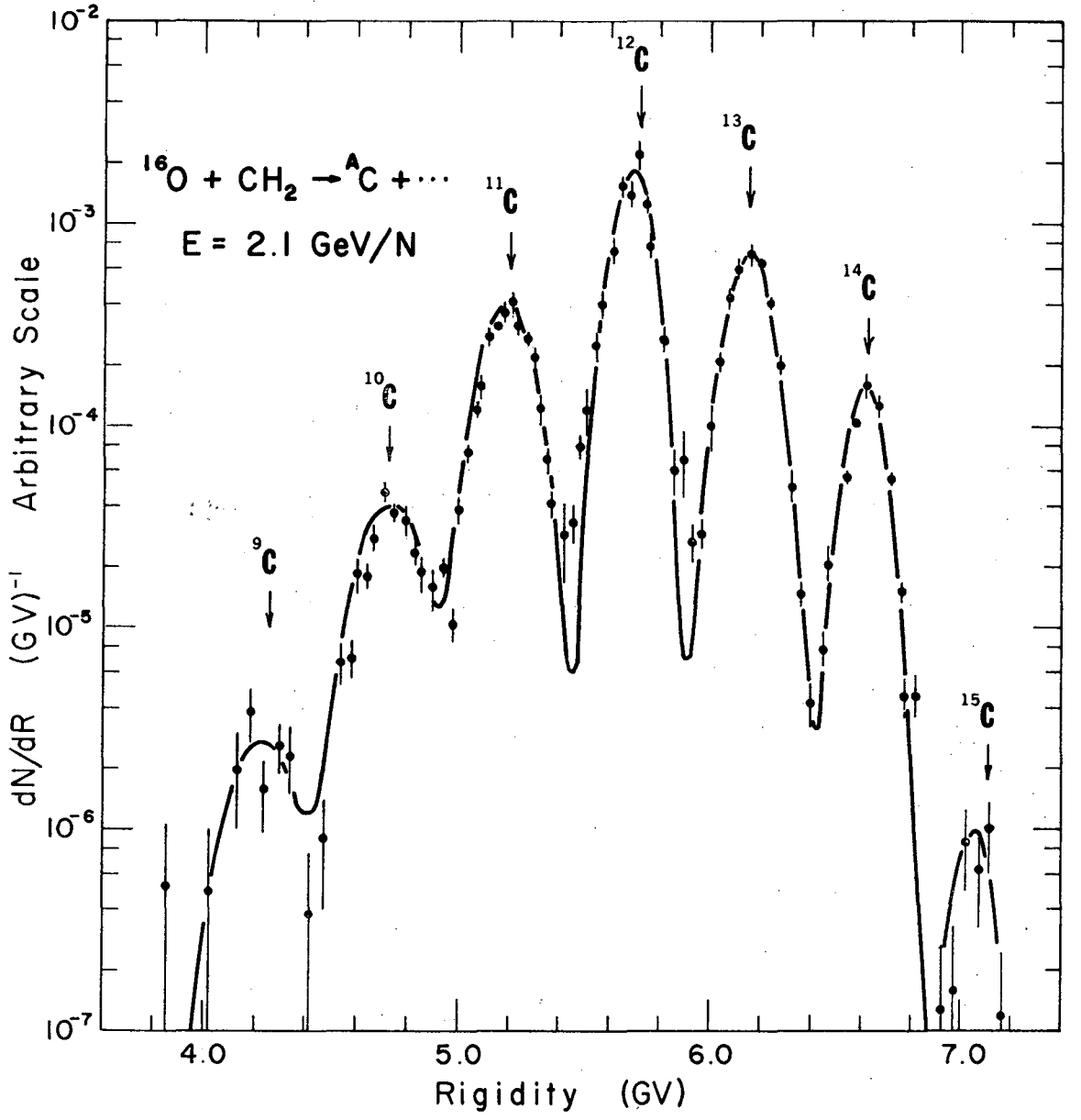

XBL 753-410A

Figure 5

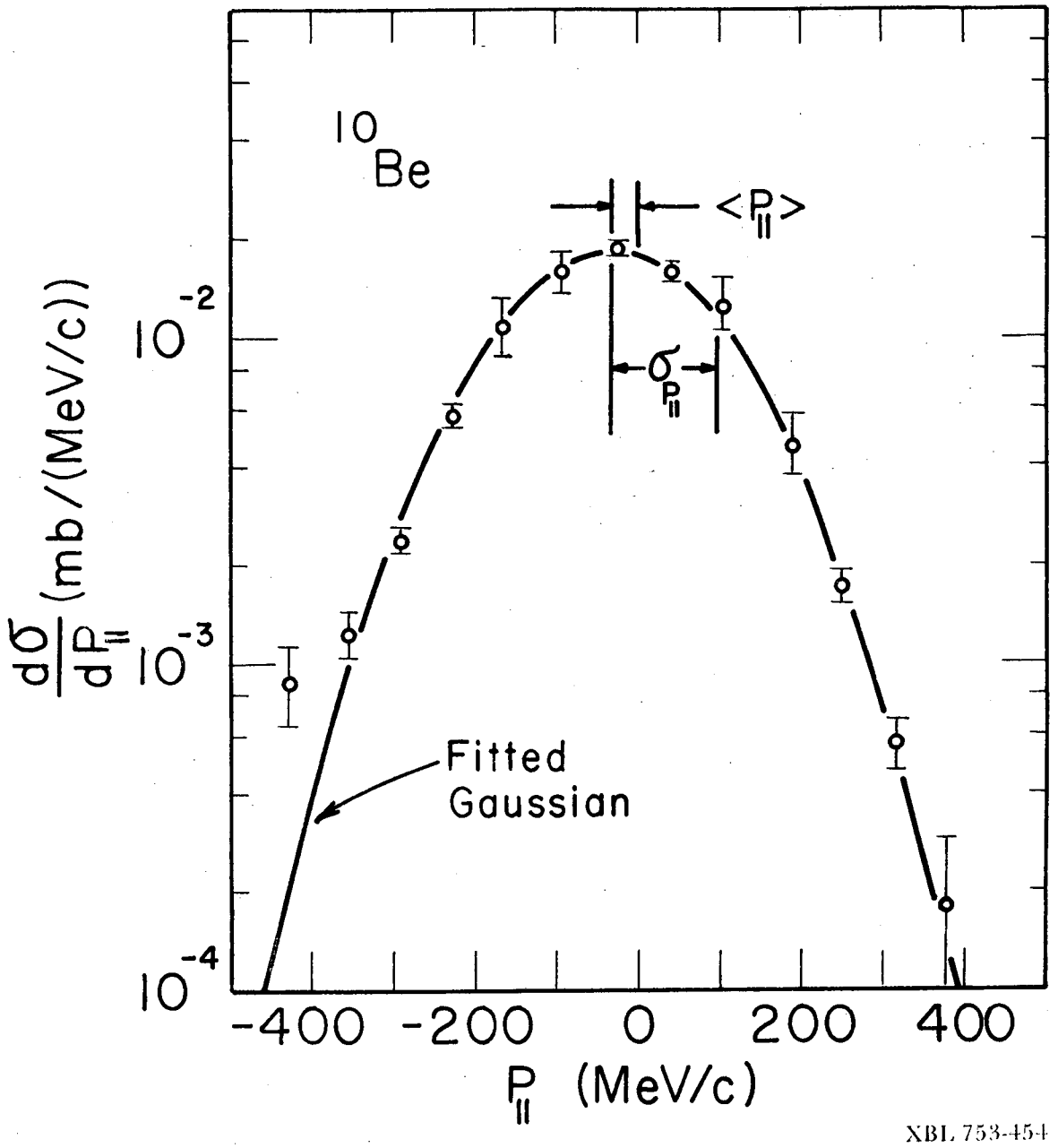

XBL 753-454

Figure 6

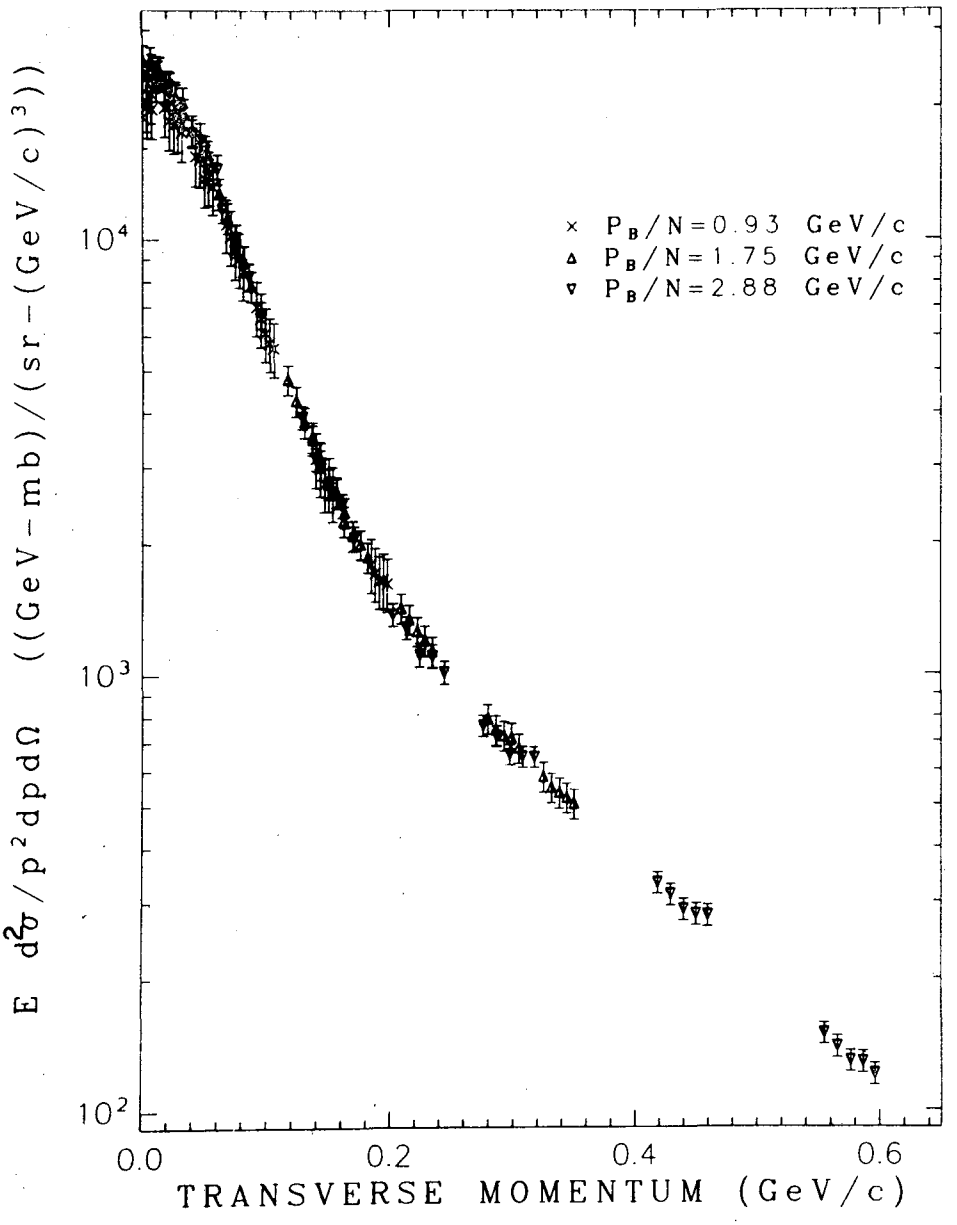

XBL 778-2602A

Figure 7

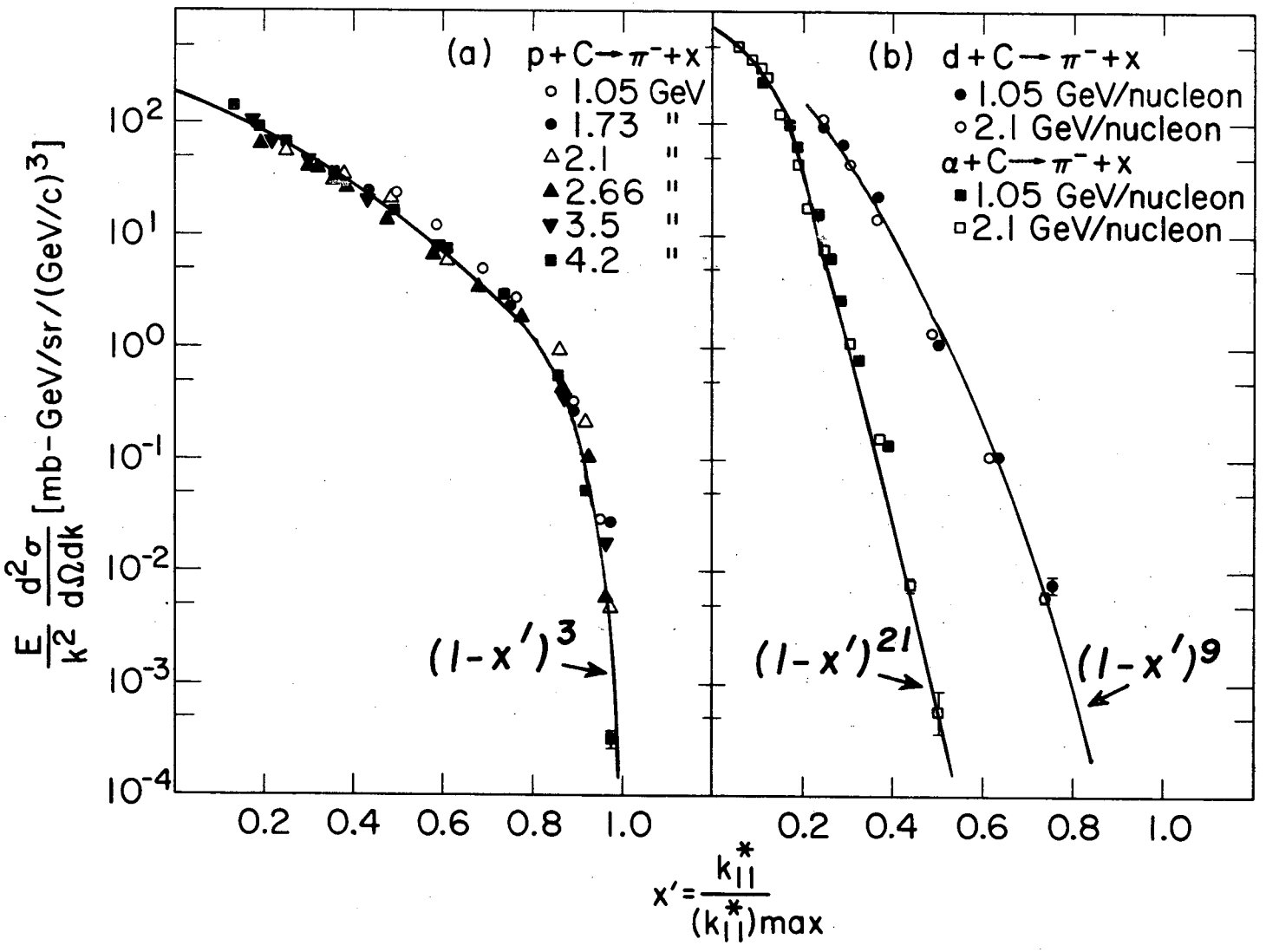

Figure 8

XBL 748-3896A

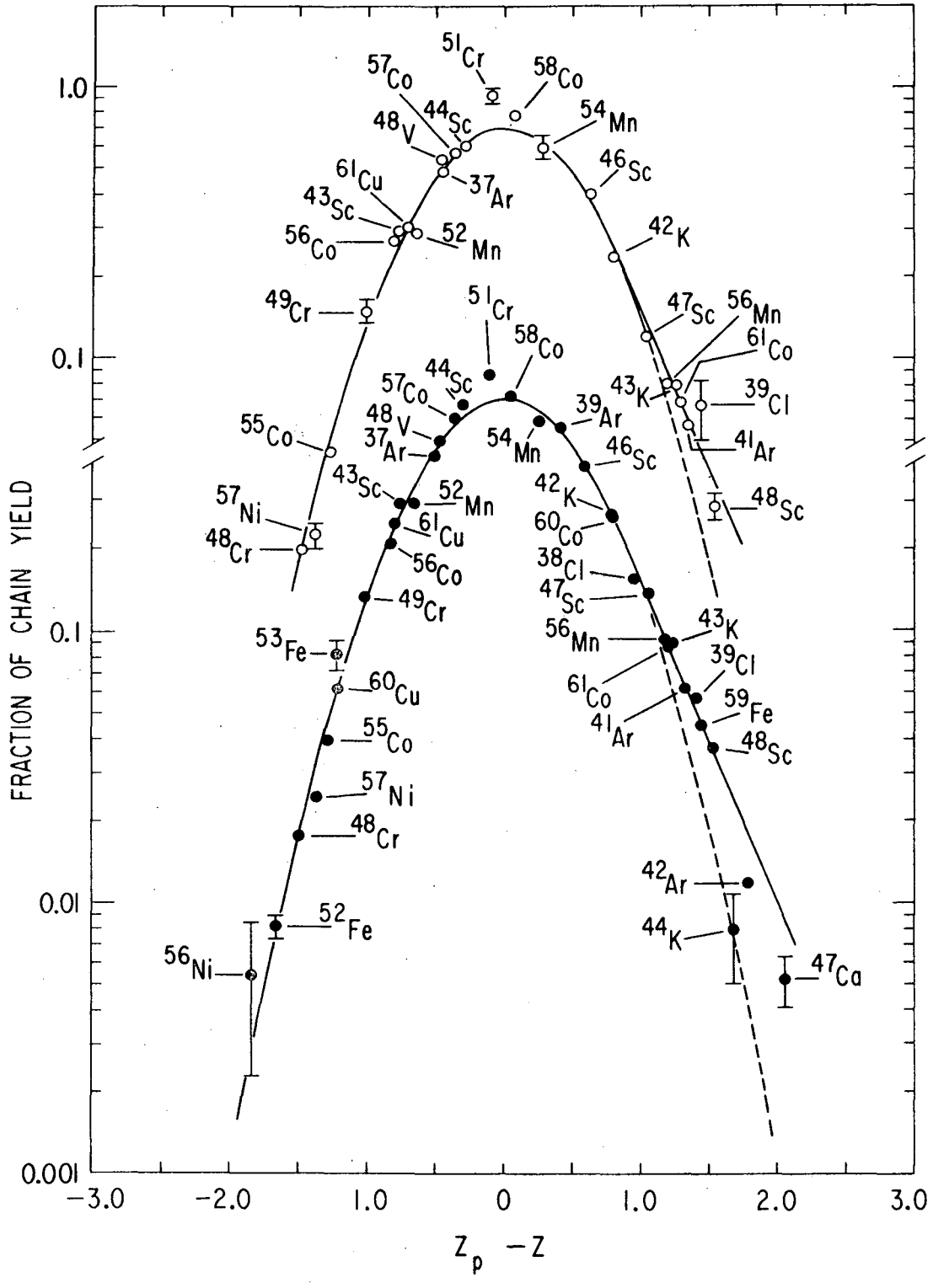

XBL 782-7153

Figure 9

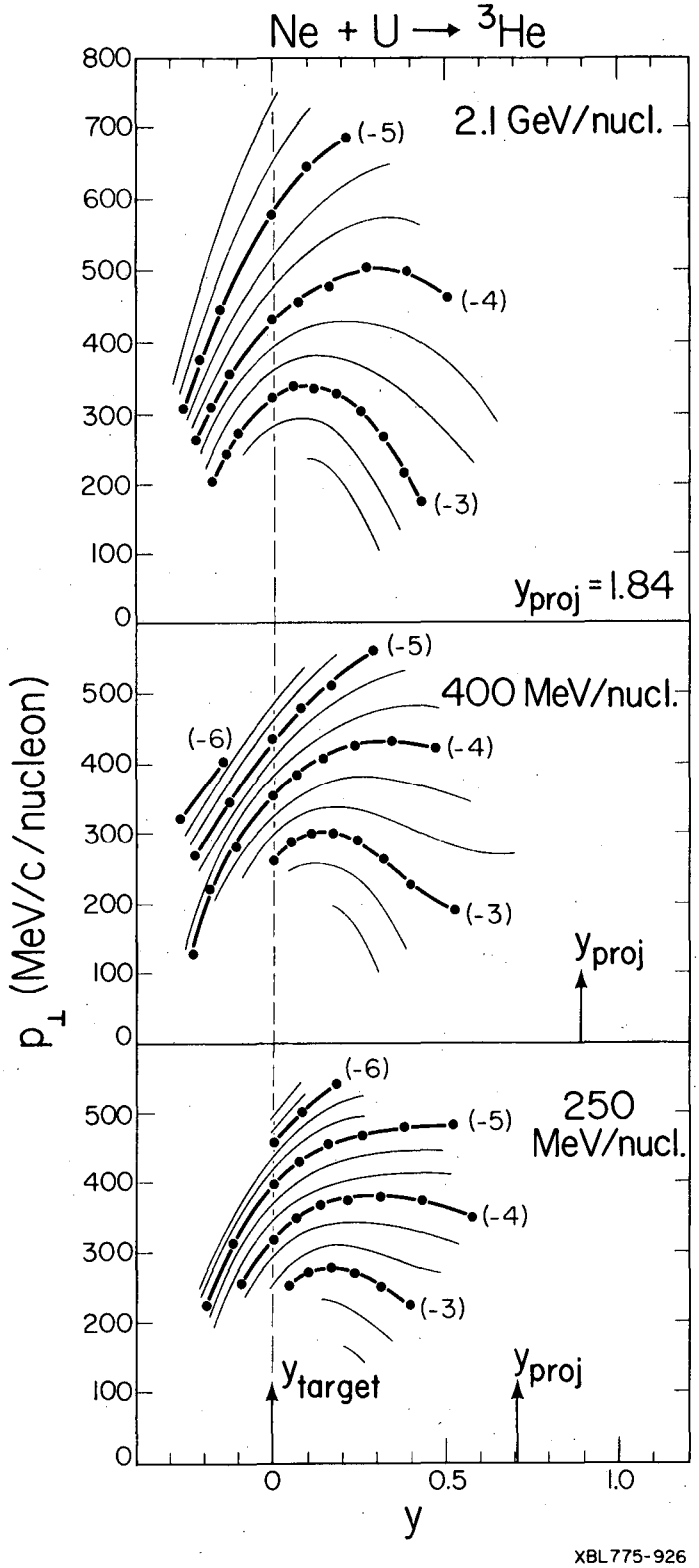
Ne + U → 3He
2.1 GeV/nucl.
(-5)
(-4)
(-3)
yproj = 1.84
400 MeV/nucl.
(-6)
(-5)
(-4)
(-3)
yproj
250 MeV/nucl.
(-6)
(-5)
(-4)
(-3)
ytarget
yproj
pT (MeV/c/nucleon)
y
0
0.5
1.0
XBL775-926

Figure 10

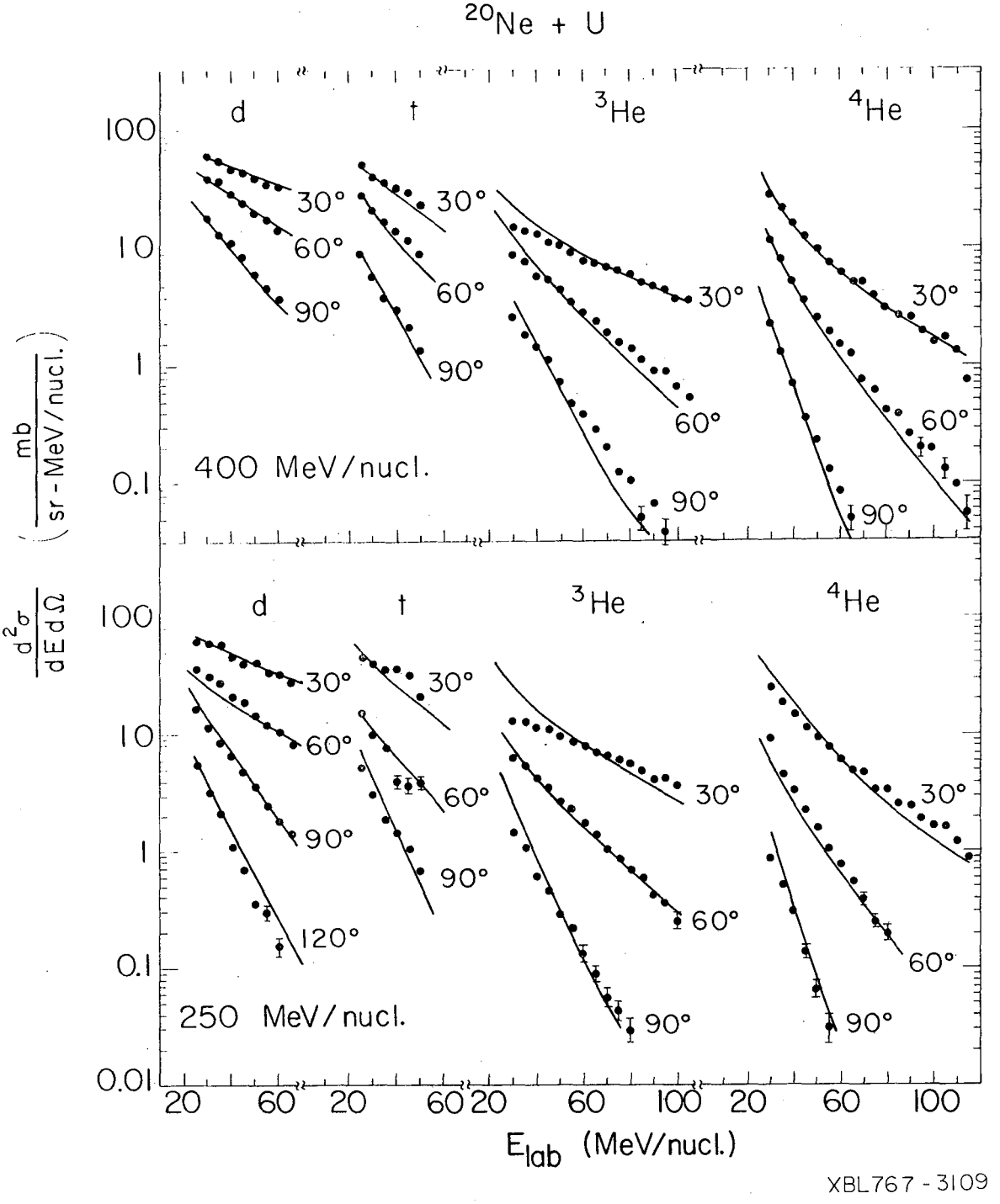
^{20}Ne + U
d
t
^{3}He
^{4}He
400 MeV/nucl.
250 MeV/nucl.
30°
60°
90°
120°
$\frac{d^2\sigma}{dE\,d\Omega}$ $\left(\frac{mb}{sr\text{-}MeV/nucl.}\right)$
100
10
1
0.1
0.01
20
60
100
E_{lab} (MeV/nucl.)
XBL767-3109

Figure 11

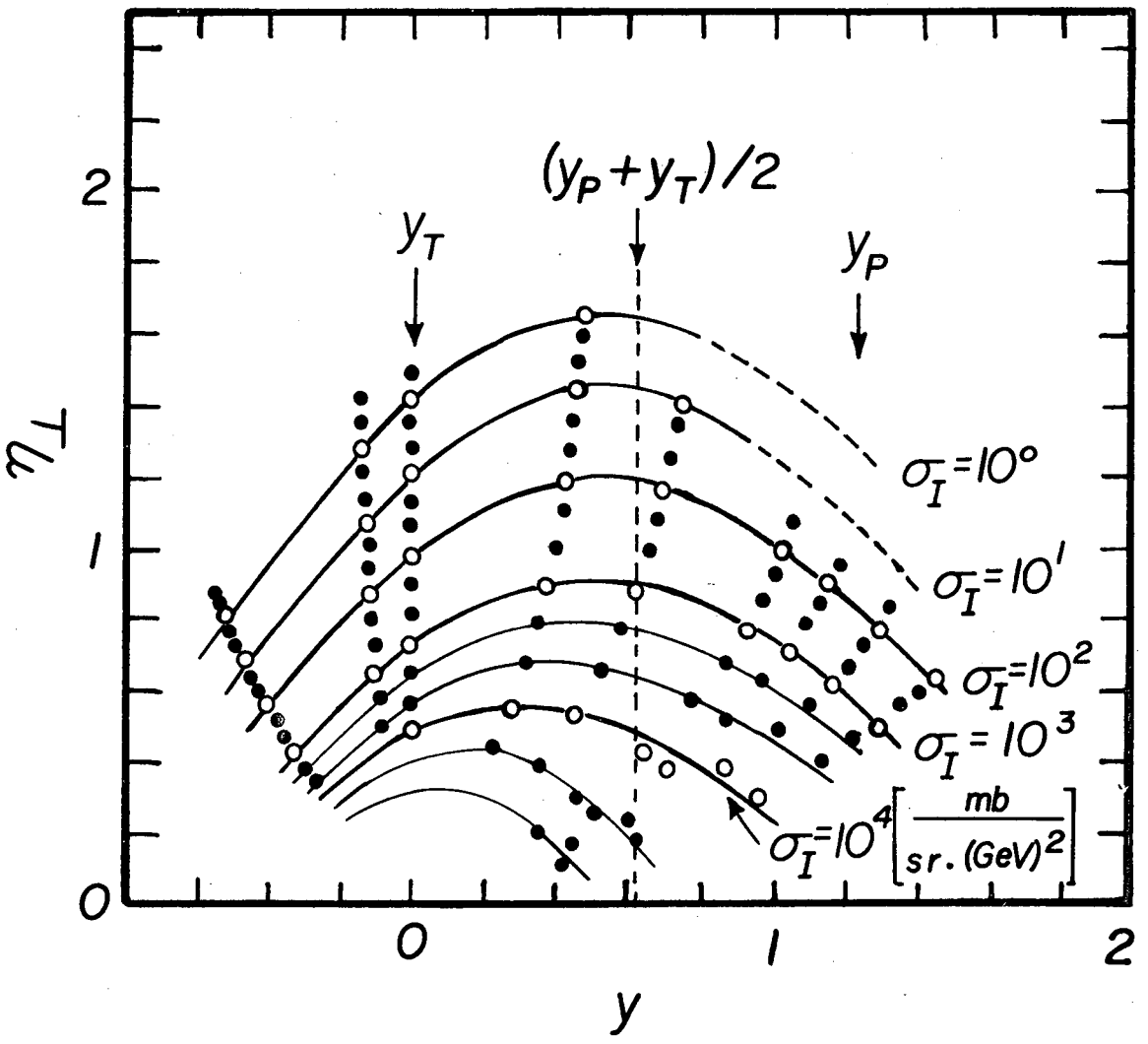

XBL 781-6749

Figure 12

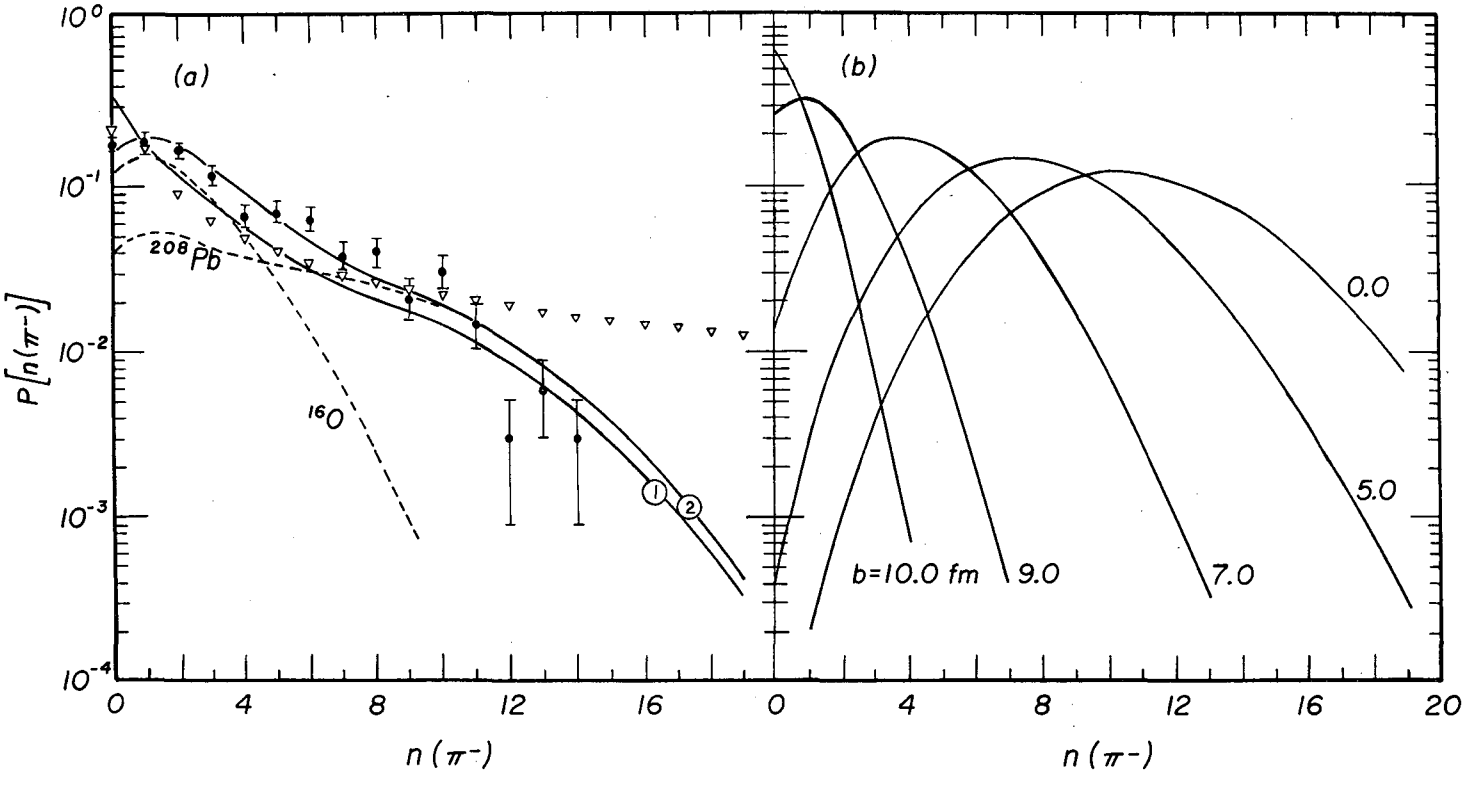

XBL 781-6751

Figure 13

TECHNICAL INFORMATION DEPARTMENT
LAWRENCE BERKELEY LABORATORY
UNIVERSITY OF CALIFORNIA
BERKELEY, CALIFORNIA 94720